

6-26-2015

Adsorption Selectivity of Cations in Constrained Environments

Maria Oba

maria.oba.mie.u@gmail.com

Recommended Citation

Oba, Maria, "Adsorption Selectivity of Cations in Constrained Environments" (2015). *Master's Theses*. 781.
https://opencommons.uconn.edu/gs_theses/781

This work is brought to you for free and open access by the University of Connecticut Graduate School at OpenCommons@UConn. It has been accepted for inclusion in Master's Theses by an authorized administrator of OpenCommons@UConn. For more information, please contact opencommons@uconn.edu.

Adsorption Selectivity of Cations in Constrained Environments

Maria Oba

B.S., Mie University, Japan, 2013

A Thesis

Submitted in Partial Fulfillment of the

Requirements for the Degree of

Master of Science

at the

University of Connecticut

2015

Copyright by

Maria Oba

[2015]

APPROVAL PAGE

Masters of Science Thesis

Adsorption Selectivity of Cations in Constrained Environments

Presented by

Maria Oba, B.S.

Major
Advisor

Cristian P. Schulthess

Associate
Advisor

Thomas F. Morris

Associate
Advisor

Chad P. Johnston

University of Connecticut

2015

Acknowledgements

First of all, I would like to express my sincere gratitude to my advisor, **Cristian Schulthess**, for giving me such a great opportunity to work on this project. It was amazing to find out what small ions are doing in the nanometers scale world. And thank you very much for guiding me through the whole time during my Master's degree. When I first started working with him I was so surprised to find out how smart he is. He taught me many things and I was greatly inspired by him. The time that I spent with my advisor will stay forever with me.

I would like to thank my associate advisor **Tom Morris** who was always cooperative and very open minded. Especially, I thank him for taking an interest in this project, even when the subject was not his major field. When I started my Master's degree my English was not very good as it is now and I remember that he always encouraged me by saying that "language is taught". Thank you very much for being supportive.

I would like to thank my associate advisor **Chad Johnston** for helping and giving me a piece of advice whenever I needed it. He always showed me his fascinating molecular dynamics simulations that inspired me a lot. I'm hoping that I can do something similar to his work and I thank him for giving me those future ideas.

I would like to thank the entire department for having me as a Master student. I know that all the small supports made me who I am today. Especially, I would like to thank **Christine Strand**, a secretary in our department, for being very kind and very supportive. She was always very polite and heartwarming person and I liked her so much.

I would like to thank my wonderful family, especially my parents **Hiroyuki Oba** and **Chizuko Oba** who were always kind and supportive.

Finally, I would like to thank my best friend and my life long partner in Japan. Whenever I was willing to do something, this person always pushed for me and encouraged me. I don't think there are many people who can do the same thing and I appreciate it so much.

Thank you, Lord, for always being there for me.

Table of Contents

Chapter 1. Introduction to NISE Effect and Ion-Exchange Modeling	1
1.1. Introduction to Research Back Ground	2
<i>1.1.1. The Importance of Ion-Exchange</i>	
<i>1.1.2. The Effect of Physical Properties on Chemical Adsorption</i>	
<i>1.1.3. The Adsorption Mechanism</i>	
<i>1.1.4. Ion-Exchange Modeling</i>	
<i>1.1.5. Cation Properties</i>	
1.2. Introduction to Zeolites	9
<i>1.2.1. History of Zeolites</i>	
<i>1.2.2. Structure of Zeolites</i>	
<i>1.2.3. Properties of Zeolites</i>	
<i>1.2.4. ZSM-5 Description</i>	
1.3. Introduction to Montmorillonite	14
1.4. The Objectives of the Study	17
References	20
 Chapter 2. Adsorption Selectivity of Alkali Metals on ZSM-5 and Determination of Adsorption Strength by Ion-Exchange Modeling	 24
Abstract	25
2.1. Introduction	26
2.2. Materials and Methods	28
2.3. Results	31
<i>2.3.1. Impact of Aluminum Sites on Sodium Adsorption</i>	
<i>2.3.2. Native Concentrations in ZSM-5</i>	
<i>2.3.3. Evaluation of Adsorption Maxima (Γ_{max})</i>	
<i>2.3.4. Multi-Site Ion-Exchange Adsorption Modeling</i>	
2.4. Discussion	40
<i>2.4.1. Impact of Aluminum Sites on Sodium Adsorption</i>	
<i>2.4.2. Evaluation of Adsorption Maxima (Γ_{max})</i>	

2.4.3. <i>Multi-Site Ion-Exchange Adsorption Modeling</i>	
2.4.4. <i>Impact of Hydration Enthalpy on Equilibrium Constant</i>	
2.5. Conclusions	49
References	51
Chapter 3. Cation Retention by Montmorillonite in Constrained Environments	53
Abstract	54
3.1. Introduction	54
3.2. Materials and Methods	56
3.2.1. <i>Column Study</i>	
3.2.2. <i>Suspension Study</i>	
3.3. Results	62
3.3.1. <i>Native Concentrations in Montmorillonite Clay Minerals</i>	
3.3.2. <i>Clay Packing Density</i>	
3.3.3. <i>Cation Adsorption on Montmorillonite</i>	
3.4. Discussion	68
3.4.1. <i>Native Concentrations in Montmorillonite Clay Minerals</i>	
3.4.2. <i>Cation Adsorption on Montmorillonite</i>	
3.5. Conclusions	73
References	75
Addendum 1. Additional Supporting Data	77
Addendum 2. Raw Data for Chapter Figures	86

Adsorption Selectivity of Cations in Constrained Environments

Maria Oba, M.S.
University of Connecticut, 2015

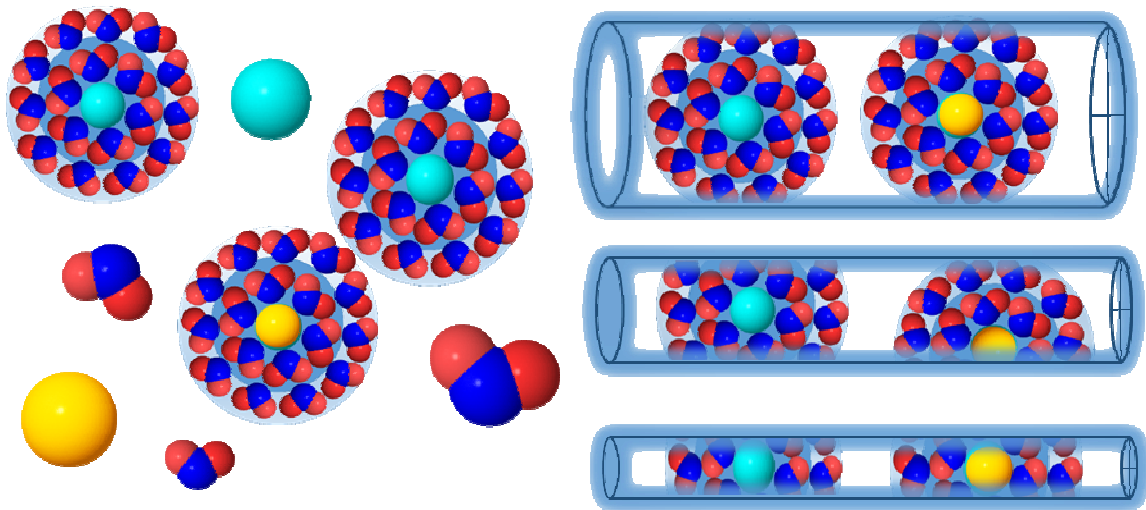
The adsorption selectivity of cations is greatly influenced by the physical properties of the adsorbent. Different sizes of the pore channels of zeolites can have a significant effect on cation adsorption capacity. The weakly hydrated ions may dehydrate and adsorb strongly onto mineral surfaces via inner-sphere complexes in zeolites with small pore channels. This phenomenon is called the nanopore inner-sphere enhancement (NISE) effect. The adsorption selectivity of Cs^+ , K^+ , and Na^+ alkali metals on the small pore channels of a ZSM-5 zeolite was studied by collecting the adsorption envelopes and analyzing the data with adsorption modeling. The adsorption of alkali metals increased on ZSM-5 with high aluminum content and the adsorption sites were mainly controlled by aluminum adsorption sites. Four adsorption sites were observed from these adsorption envelopes. The adsorption data were described using a simple, net-neutral, ion-exchange model with four reaction sites. The data were well predicted by the model, which described the adsorption strength of each cation by its equilibrium constant (pK). The adsorption of alkali metals had a selectivity sequence of $\text{Cs}^+ > \text{K}^+ > \text{Na}^+$ for inner-sphere complexes. The adsorption strength (pK) of each cation had a strong correlation with the hydration enthalpy ($\Delta H_{\text{hyd}}^\circ$), indicating that the free energy of the adsorption reaction (ΔG°) is greatly influenced by the cation's hydration enthalpy. A shift in the adsorption strength of these cations on ZSM-5 was also observed and was described in terms of their solubility interactions inside the pore channels.

The adsorption selectivity of alkali metals was also studied on montmorillonite clay minerals in constrained and non-constrained environments. Montmorillonite clay minerals were placed in a stainless-steel container to limit the expansion of the interlayer and to create a constrained environment, or were suspended in a container for free expansion of the interlayer and to create a non-constrained environment. The dominant native cation concentrations present in the montmorillonite clay minerals were Na^+ and Ca^{2+} . Cations are likely to form weakly held OS complexes in non-constrained environments, and their adsorption depends greatly on their initial concentrations, ionic hydration diameters, ionic diameters and valences. The adsorption of Na^+ cations increased its adsorption strength in the constrained environments, while the adsorption of the other cations decreased slightly or did not show any changes. This enhanced retention behavior of Na^+ cations in constrained environments suggests that the physical NISE phenomena previously observed on zeolites may also be applicable to montmorillonite clay minerals.

Chapter 1

Introduction to NISE Effect and

Ion-Exchange Modeling



1.1. Introduction to Research Back Ground

1.1.1. The Importance of Ion-Exchange

On March 11, 2012, the Fukushima Daiichi Nuclear Power Plant (FDNPP) was seriously damaged by a catastrophic earthquake and tsunami in Japan. The explosion of nuclear furnaces led to a great emission of radioactive cesium (^{137}Cs , ^{134}Cs) that spread widely throughout the central eastern region of Japan. Radioactive cesium is highly soluble in water as an alkali metal ion and has a long half-life (30.17 years for ^{137}Cs , 2.07 years for ^{134}Cs). Radioactive cesium is easily assimilated by living organisms, and is a threat to the food chain and the human body (Cremers et al., 1988; Bostick et al., 2002; Tsukada et al., 2002).

A serious problem that followed the emission of radioactive cesium was the contamination of soils in farms, forests and grasslands around FDNPP and neighboring prefectures (Kinoshita et al., 2011; Yasunari et al., 2011). Studies on vertical soil profiles showed that high concentration levels of radioactive cesium were accumulated at the very top surface of soils in Fukushima Prefecture (Ohno et al., 2012; Tanaka et al., 2012). Spectroscopic studies of radioactive cesium in soils showed a high affinity of this element to clay minerals, whose structures are composed of layers of shared silicate tetrahedral and aluminum octahedral sheets (Cha et al., 2006). In clay minerals, there are interlayer spaces between the layers where non-framework cations are retained. Radioactive cesium is known to ion exchange with cations in the interlayer, forming a tight bond with the surface functional groups (Bostick et al., 2002).

1.1.2. The Effect of Physical Properties on Chemical Adsorption

Various efforts were made to remediate the radioactive cesium from the contaminated soils. However, due to the strong adsorption of radioactive cesium on clay minerals, there are no practical remediation processes that can be applied in the field. In addition, the adsorption mechanism processes of radioactive cesium remains unexplained in many respects. Accordingly, the elucidation of the adsorption mechanism is an urgent topic. In recent years, there is a growing awareness that ion exchange is controlled by the physical effects of the solid phase. For example, Adam et al. (2015) showed that the strong retention of Cs^+ occurs in the frayed edge of illites.

In general, the retention behavior of ions is strongly dependent on chemical properties of the solid and liquid phase, including mineralogy, pH, ionic strength and competitive cations. However, Ferreira and Schulthess (2011) have shown that the chemical adsorption of ions can be affected by the physical properties of the solid phase. They studied the effectiveness in the adsorption selectively of three cations (Na^+ , K^+ , and Ca^{2+}) on the porous aluminosilicate zeolite mineral. In their experiments, four types of zeolites differing in pore size dimensions (small, medium and large) were chosen as cation adsorbents. The zeolite with large pores had much lower adsorption values than the other three zeolites for all the cations studied. These results indicated that the chemical adsorption selectively of ions on zeolites is greatly influenced by the physical properties of its pore channel dimensions. They noted that the physical effect on cation adsorption mechanisms should be taken as an important phenomenon, and they named this phenomenon the nanopore inner sphere enhancement (NISE) effect.

Zeolites are hydrated aluminosilicate minerals compositionally similar to clay minerals. The significant difference between these two minerals is the physical properties of the d-spacing inside the framework structures. Zeolites have pore channels in the structure where cations and water molecules adsorb through ion exchange. These pore channels are rigid due to the chained structure of zeolites, and there are limitations to the size of the ions that can fit inside the pore channels (Helfferich, 1962). In contrast, clay minerals have planar interlayers where cations and water molecules are also adsorbed through ion exchange. Without changing the original structure of the clay minerals, these interlayers can expand and increase in size, depending on the radius of the ion adsorbed and its degree of hydration. The swelling properties of the minerals can be seen in 2:1 clay minerals such as vermiculite, bentonite and montmorillonite. As a representative of clay minerals, the structure and properties of montmorillonite are described later in this chapter.

1.1.3. The Adsorption Mechanism

Bioavailability and the mobility of inorganic ions are greatly affected by the retention of ions on the solid surface (Violante et al., 2010). Ions and molecules transported in the subsurface interact with mineral surfaces creating a bond at the solid-liquid interface. This process removes contaminants from the mobile aqueous phase and decreases the risk imposed by toxic elements. However, it also restricts nutrient availability for plant uptake (Bray, 1954). Accordingly, it is important to understand the processes of retention by which ions are removed from solution and how strongly they are immobilized.

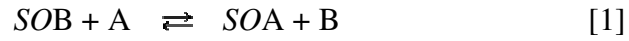
Ions in solution are retained by mineral surfaces by different reactions. There are two fundamental interactions: electrostatic attraction and chemical adsorption. The electrostatic attraction involves the columbic interactions forming a bond between the mineral surface and water molecules surrounding the ions, and this formation is referred to as an outer-sphere (OS) complex. This columbic interaction is the electrical attraction of oppositely charged species, such as a positively charged cation with a negatively charged surface site. In the formation of this outer-sphere complex, there is always at least one water molecule involved between the ion and the solid surface. Thus, the ion is only weakly held by electrostatic attraction and is easily replaced by other similarly charged ions. In contrast, chemical adsorption, which refers to inner-sphere (IS) complexes, does not involve intervening water molecules. The ion directly forms a chemical bond with the surface functional group regardless of the surface charge. Therefore, inner-sphere complexes can increase, reduce, neutralize or reverses the original charge and any charge imbalance is subsequently neutralized by other ions. Inner-sphere complexes can be monodentate (bound to one surface site) or bidentate (bound to two surface sites), and they can be mononuclear (one surface atom involved) or binuclear (two surface atoms involved) (Sposito, 1989).

1.1.4. Ion-Exchange Modeling

Adsorption modeling has become one of the most common techniques to predict the phenomena of adsorption reactions. Various thermodynamic approaches have been proposed to understand ion exchange reaction processes (Kerr, 1928; Vanselow, 1932; Glueckauf, 1949; Gaines and Thomas, 1953). Accordingly, it is important to determine which reaction is applicable to describe the adsorption reaction through modeling.

The ion exchange models were among the earliest adsorption models that described the interchange between an ion in solution and another ion on the solid surface. Ion exchange reactions follow the law of chemical equilibria, which quantifies the bond strength between the exchangeable cations adsorbed on mineral surfaces (Robinson, 1962; Schulthess and Sparks, 1991). Generally, they are based on a constant exchange capacity and a completely neutral solid phase.

The most simplified ion exchange reaction is:



where SO represents the functional group on the solid surface, and A and B are ions in the aqueous phase. The equilibrium constant can be defined as:

$$K = \frac{\{SOA\}(B)}{\{SOB\}(A)} \quad [2]$$

where $\{SOA\}$ and $\{SOB\}$ represent the concentration of sites adsorbing component A and B, (B) and (A) are the activity of A and B in the aqueous phase, and K is the equilibrium constant for the reaction. From mass balance principles, the total number of sites (Γ_{max}) is defined as:

$$\Gamma_{max} = \Gamma_A + \Gamma_B \quad [3]$$

where Γ_A and Γ_B equal $\{SOA\}$ and $\{SOB\}$, respectively. From Equation [2] the adsorption of compound A can be predicted as:

$$\Gamma_A = \frac{\Gamma_{max} K (A)}{(B) + K (A)} \quad [4]$$

The ion exchange model derived from Equations [1] to [4] is the most basic and simple version of these types of models. This model assumes an ion exchange reaction of only two monovalent ions in the aqueous phase, competing against each other for adsorption on only one surface site in the solid phase. However, ion exchange reactions can occur in multiple adsorption sites and with many competing ions. Each adsorption site has an independent ion exchange reaction with its own unique K value. Furthermore, competitive adsorption generates multiple reactions. Equation [4] is for a single ion-exchange reaction that is easy to solve by hand. However, a model with multi-adsorption sites yields many equations that must be solved simultaneously. To simultaneously solve complicated algebraic equations, computer software has been developed, such as IExFit, which is distributed via www.alfisol.com.

1.1.5. Cation Properties

The retention of monovalent cations is frequently described as weakly adsorbing OS complexes. However, in constrained environments such as in nanopores, the monovalent cation dehydrates its hydration shell and results in a significantly stronger IS complex instead. This physical effect on adsorption is due to the NISE effect (Schulthess et al., 2011).

Monovalent cations of alkaline metals are commonly found in a wide variety of ionic compounds, typically as salts. Sodium (Na^+) has a great influence in the soil environment, and it is the sixth most abundant element (2.6%) of the Earth's crust. For example, salt-affected soils (sodic soils) are causing great loss to agricultural productivity in 7% of the total land around the globe (Wakeel, 2013). Potassium (K^+) is also an abundant element, consisting of around 2.4% of the Earth's crust. Comparatively

high levels of potassium are found in most soil minerals and are held rigidly as part of the primary minerals or in a fixed form in secondary minerals (non-exchangeable K^+). Plants uptake large amounts of exchangeable K^+ cations, however, it is readily lost by leaching due to the weak retention of its OS complexes on mineral surfaces (Sparks, 2000). Cesium (Cs^+) is considerably rarer on the Earth's crust. However, radioactive cesium (^{137}Cs) released from nuclear power plant accidents has a long half-life of 30.17 years and is toxic to humans in elevated concentrations.

Alkaline salts are highly soluble due to their large entropies of solution, and their heats of solution are often endothermic (Djamali et al., 2009). In solution, alkali metals are weakly hydrated and the heats of hydration are small (Smith, 1977). The smaller the cation, the greater is the degree of its hydration (Table 1-1).

Table 1-1. Properties of alkali metal cations: ionic diameter (Mähler and Persson, 2012) and hydrated diameter (Gast, 1977).

Cations	Ionic Diameter, nm	Hydrated Diameter, nm
Na^+	0.214	0.716
K^+	0.286	0.662
Cs^+	0.356	0.658

1.2. Introduction to Zeolites

1.2.1. History of Zeolites

The commercial use of zeolites is wide ranging due to their unique adsorption, diffusion, and catalytic properties. Major uses are petrol chemical cracking and in separation processes for gasses and solvents (Vermeiren and Gilson, 2009). Zeolites are also used in soils to enhance cation exchange capacity and soil moisture in agricultural fields (Peng et al., 1995).

Zeolites are naturally occurring hydrated aluminosilicate minerals compositionally similar to clay minerals. The most common natural zeolites are formed by alteration of glass-rich volcanic rocks (tuffs) with fresh water in playa lakes or seawater (Badillo-Almaraz et al., 2003).

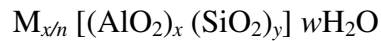
Zeolites were originally discovered in the 18th century by the Swedish mineralogist Axel Fredrik Cronstedt, who noticed that the stone bubbled and danced in boiling water (Cronstedt, 1756). Zeolites were thus also known as “boiling stones” for distillation procedures. In 1840, Damour discovered the reversible hydration-dehydration character of zeolites. This property provided an important use of zeolites as a drying agent for liquids and gases. Later, the cation exchange capacity of zeolite was discovered. Grandjean (1909) observed the phenomenon of selective adsorption of ammonia on zeolite. Thus, zeolites are now also used as molecular sieves. Since the discovery of the first zeolite, approximately 40 different natural zeolite species have been found.

Natural zeolites lack uniformity in their pore sizes and are more likely to contain contaminants (Virta, 2000). The number and available amounts of natural zeolites of

consistent quality are limited. In the late 1940s and early 1950s, the synthesis of zeolites was developed. The number of synthetic zeolites currently surpasses 130 different types as classified by the International Zeolite Association (IZA; <http://www.iza-online.org/>). The zeolites are assigned three letter codes based on their framework topology irrespective of composition. Illustrative codes are LTA for Linde zeolite A, FAU for faujasite, MOR for the mordenite, MFI for ZSM-5, and AFI for the alumina phosphate zeolites. In this study ZSM-5 was used as an adsorbent. Detail properties of ZSM-5 are discussed later in this chapter.

1.2.2. Structure of Zeolites

In general, the structure of zeolites consists of three dimensional tetrahedral frameworks of covalently bonded TO_4 units. The framework T atom is usually a silicate (Si) or aluminum (Al) atom (Kitagawa et al., 2004). If the framework atom is Si, then the unit will be electrically neutral, while an Al atom results in a negative charge site. This charge has to be compensated to yield an electrically neutral crystal. Hence, the substitution of a Si atom by an Al atom requires the presence of a non-framework cation like hydrogen (H^+), sodium (Na^+) or potassium (K^+) to neutralize the charge (Speight and James, 1980). The empirical formula of zeolites can be expressed as:



where n is the valence of the charge balancing cation M, w is the number of water molecules for each unit cell, x and y are the total number of tetrahedra per unit cell.

1.2.3. Properties of Zeolites

Zeolites are used in many different fields due to their unique properties as adsorbents. The structural surface area of zeolites with different dimensions of 3D

channels reaches several hundred square meters per gram. The adsorption of ions can occur on the outer surface of the mineral or the inner surface of the nanopores of about 0.1-2 nm diameter running throughout the material. The pore size properties of zeolites have extraordinary effects on adsorption processes. Ions with diameters larger than the zeolite's pore size cannot pass through the entrance of the channel to absorb, which is why zeolites are also known as molecular sieves and are particularly useful in separating organic molecules (Breck, 1974).

The adsorption capacity also depends on the polarity of both the absorbent and adsorbate. The $\text{SiO}_2/\text{Al}_2\text{O}_3$ ratio in the zeolite structure impacts the charge and determines the ions that can absorb in the zeolite. The substitution of Si^{4+} for Al^{3+} causes an imbalance in the structure characterized by an excess of negative charges (Speight and James, 1980).

Another property of zeolites is ion-exchange. Hydrated cations within the pores of the zeolite are weakly attached and ready to exchange with other cations in the bulk solution. These cations are easily interchanged and give the zeolite a high ion exchange capacity. Through this exchange, other metal cations can be introduced into the zeolite structure and thus modify their catalytic properties or molecular sieve properties (Breck and Donald, 1974).

1.2.4. ZSM-5 Description

ZSM-5 is a synthetic zeolite classified as MFI framework topology (for Mordenite Framework Inverted) and its chemical formula per unit cell is $(\text{H},\text{Na})_n[\text{Al}_n\text{Si}_{96-n}\text{O}_{192}]$. The name ZSM-5 refers to Zeolite Socony Mobil-5. ZSM-5 was made by Argauer and Landolt in 1972 for catalytic processes, such as catalytic cracking

of hydrocarbons and hydrocracking (Argauer and Landolt, 1972). The special properties of ZSM-5 are the high silicate content and thermally stable framework structure. The framework structure of ZSM-5 consists of interconnecting straight and zigzag channels building three directional pore channels (Figure 1-1). The size of the pore is 0.51 × 0.55 nm for straight channels and 0.53 × 0.56 nm for zigzag channels (Database of Zeolite Structures: <http://www.iza-structure.org/databases/>). The diameter of the pore channels are approximately the diameter of hydrated cations and it has extraordinary effects on its cation selectivity. The studies conducted by Schulthess et al. (2011) and Ferreira and Schulthess (2011) have shown that the physical pore dimension of ZSM-5 enhances the adsorption of monovalent cations. When a hydrated monovalent cation enters the pore channels, it sheds its hydration sphere to adsorb as a strong inner-sphere complex. Note that monovalent cations are generally known to form very weak outer-sphere complexes on mineral surfaces.

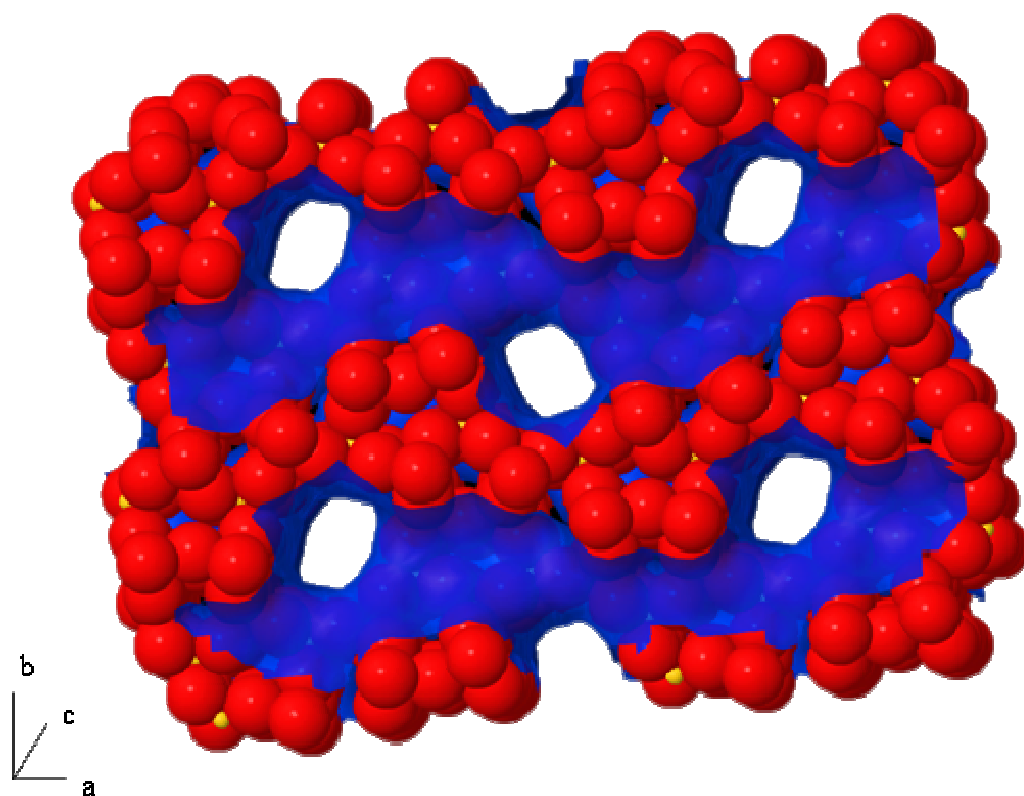


Figure 1-1. Structure of ZSM-5. Oxygen atoms shown in red, Si and Al atoms shown in yellow, and internal channel surfaces shown in blue. Straight channels are shown in c-axis directions and zigzag channels are shown in a-axis directions. Image generated by Jmol software (<http://www.iza-structure.org/databases/>).

1.3. Introduction to Montmorillonite

Montmorillonite is a well-known aluminosilicate clay mineral commonly found in soils. The name “montmorillonite” was given by Damour and Salvétat (1847) who described a rose-red clay-like mineral, forming a nest in brown clay at Montmorillon in France (Hauser, 1953). The montmorillonite is formed by weathering of eruptive rock materials, such as volcanic ash and tuffs. The structure of montmorillonite consists of two tetrahedral silica sheets surrounding an octahedral alumina sheet (Figure 1-2), and its typical chemical formula per unit cell is $(\text{Na}, \text{Ca})_x(\text{Al}, \text{Mg})_2(\text{OH})_2[\text{Si}_2\text{O}_5]_2 \cdot n\text{H}_2\text{O}$. The thickness of each layer is approximately 0.96 nm and the diameter is around 300 nm (Ishida, 2011).

Within these layers, there are extensive isomorphic substitutions, such as Al^{3+} replaced by Mg^{2+} , and Si^{4+} replaced by Al^{3+} . These substitutions cause an imbalance in the structure, which results in charge deficiencies of the particles. The imbalance of the charge is balanced by the hydrated inorganic cations that are retained weakly by the electrostatic attraction in the interlayers. Typically the cations retained are Na^+ or Ca^{2+} , and these hydrated cations are exchangeable. The presence of these interlayer mono- and divalent cations weakens the attraction between the layers, allowing water molecules to enter the interlayer space and force the layers apart and the clay to swell. Water molecules are normally associated with the cation, forming hydration shells around them to complete the filling of the interlayer space. Hence, the interlayer expansion and the packing density of water molecules are affected by the density and type of cations present in the interlayer. In the case of Na^+ as the interlayer cation and in the presence of large amounts of water, the montmorillonite becomes fully expanded. The spacing of the

interlayer can reach 1.7 to 2 nm, but the typical interlayer spacing is 0.3 to 0.5 nm (Ishida, 2011). Montmorillonite has a similar composition as zeolites because montmorillonite is also known to produce zeolites through the weathering process. This occurs when there are high Na^+ concentrations in the solutions (Frankart and Herbnillio, 1970). In the large hydrated interlayers of montmorillonite, large monovalent cations such as Cs^+ cations are known to weakly adsorb electrostatically via outer-sphere complexes. The selectivity of cations is greatly influenced by the physical d-spacing of the clay interlayer.

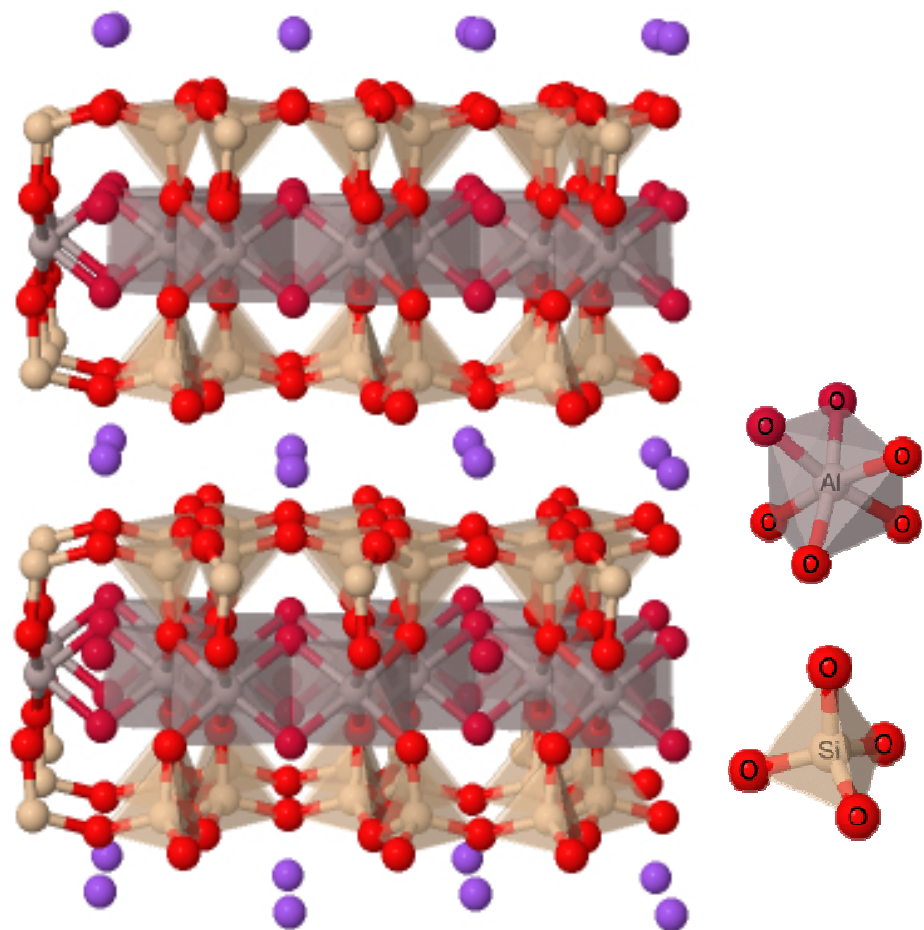


Figure 2-1. Computer models of montmorillonite showing the framework structure. Image generated by Jmol software (<https://chemlinks.beloit.edu/edetc/index.html>).

1.4. The Objectives of the Study

The application of natural zeolites has been widely used for the remediation of hazardous contaminants in the environment (Misaelides, 2011). Natural zeolites are effective at removing or immobilizing the contaminants of industrial waste and nuclear reactor accidents. The use of natural zeolites as a remediation tool was extensively studied in the previous century, and zeolites such as clinoptilolite were already being applied to immobilize radioactive cesium (Ames, 1962). Synthetically modified zeolites with strong adsorption capacities were recently introduced as reactive barriers to clean contaminated water (Bowman, 2003). The application of natural and synthetic zeolites is becoming one of the efficient materials used for environmental remediation (Misaelides, 2011). The extensive success of zeolites as a remediation tool and in industrial applications is mainly attributed to their crucial properties of high ion-exchange selectivity, high surface area, strong adsorption capacity inside the channels, and extensive structural frameworks of inter-connected pore channels (Yilmaz et al., 2012).

Recent research conducted by Schulthess et al. (2011) and Ferreira and Schulthess (2011) has shown that the different sizes of the pore channels of zeolites can have a significant effect on adsorption capacity. They studied the effectiveness in adsorption selectively of various cations (Na^+ , K^+ , Ca^{2+} and Ni^{2+}) by four types of zeolites differing in pore size dimensions (small, medium and large) as a function of pH. The zeolite with large pores had much lower adsorption values than the other three zeolites for all the cations studied. These results indicated that the chemical adsorption selectively of cations on zeolites is strongly affected by the physical properties of the channels. This phenomenon is called the nanopore inner-sphere enhancement (NISE)

effect. The NISE effect states that the weakly hydrated ions may dehydrate and adsorb strongly onto mineral surfaces via inner-sphere complexes in the constrained nanopore environment. Subsequent research using nuclear magnetic resonance (NMR) confirmed that Na^+ cations, which typically adsorbed very weakly via outer-sphere complexes, were adsorbing via a strong inner-sphere mechanism on the small pore size channels, such as those found in ZSM-5 and mordenite (Ferreira et al., 2012). The adsorption sites for Na^+ cations on the ZSM-5 zeolites are presumably aluminum adsorption sites (Breck, 1974).

The overall objective for this research project is to improve our understanding of how cations adsorb in constrained environments, such as inside the nanopores in ZSM-5 zeolite or the interlayers in montmorillonite clay minerals. More specific objectives are listed below:

- (1) Confirm that the aluminum content effects adsorption of alkali metals (Na^+ , K^+ and Cs^+) on zeolite.
- (2) Quantify the adsorption strength of these cations in a constrained environment (zeolite) using ion-exchange modeling.
- (3) Study cation adsorption on montmorillonite by controlling the dimension of the interlayer to see if there is a physical influence.

Objective (1) was accomplished by studying the single and competitive adsorption of alkali metal cations (Na^+ , K^+ and Cs^+) on ZSM-5 (Chapter 2). The adsorption of alkali metals increased with increasing amount of aluminum per unit cell in the ZSM-5 framework structure. Objective (2) was accomplished by modeling the data set from the first study of single and competitive adsorption study of alkali metal

cations (Chapters 2). The adsorption strength of cations followed the sequence of $\text{Cs}^+ > \text{K}^+ > \text{Na}^+$ and the presence of a mixture of these cations not only reduces adsorption by competition but also shifts their adsorption strength. Objective (3) was pursued with a pure phase 2:1 montmorillonite clay mineral (Chapter 3). The adsorption of cations on the clay mineral was affected by the physical impact of constrained environments.

References

- Argauer, R.J., and G.R. Landolt. 1972. Crystalline zeolite ZSM-5 and method of preparing the same. U.S. Pat. No. 3,702,886.
- Badillo-Almaraz, V., P. Trocellier, and I. Dávila-Rangel. 2003. Adsorption of aqueous Zn(II) species on synthetic zeolites. *Nuclear Instruments and Methods in Physics Research Section B: Beam Interactions with Materials and Atoms* 210:424-428.
- Bostick, B.C., M.A. Vairavamurthy, K.G. Karthikeyan, and J. Chorover. 2002. Cesium adsorption on clay minerals: An EXAFS spectroscopic investigation. *Environ. Sci. Technol.* 36:2670-2676.
- Bowman, R.S. 2003. Applications of surfactant-modified zeolites to environmental remediation. *Microporous and Mesoporous Materials* 61:43-56.
- Bray, R.H. A nutrient mobility concept of soil-plant relationships. 1954. *Soil Science* 78:9-22
- Breck, D.W. 1974. Zeolite molecular sieves: Structure, chemistry, and use. Wiley-Interscience, New York, NY.
- Gast, R.G. 1977. Surface and colloid chemistry. *In* J.B. Dixon and S.B. Weed (eds), *Minerals in Soil Environments*. Soil Science Society of America, Madison.
- Cha, H.J., M.-J. Kang, G.H. Chung, and G.S. Choi. 2006. Accumulation of ^{137}Cs in soils on different bedrock geology and textures. *J. of Radioanalytical and Nuclear Chemistry* 267:349-355.
- Cremers, A., A. Elsen, P. De Preter, and A. Maes. 1988. Quantitative analysis of radiocaesium retention in soils. *Nature* 335:247-249.
- Cronstedt, A.K. 1756. Observation and description of an unknown kind of rock to be named zeolites. *Kongl. Vetenskaps Acad. Handl. Stockholm* 17:120-123 (in Swedish).
- Damour, A. 1840. Sur le plomb gomme et sur le plomb phosphate aluminifère de Huelgoat, en Bretagne. *Annales des Mines* 17:191-202.
- Djamali, E., and J.W. Cobble. 2009. Standard state thermodynamic properties of completely dissociated hydrochloric acid and aqueous sodium hydroxide at extreme temperatures and pressures. *J. Physical Chemistry B* 113:10792-10799.
- Ergin, M., B. Kiskan, B. Gacal, and Y. Yagci. 2007. Thermally curable polystyrene via click chemistry. *Macromolecules* 40:4724-4727.

Ferreira, D.R., and C.P. Schulthess. 2011. The nanopore inner sphere enhancement effect on cation adsorption: Sodium, potassium, and calcium. *Soil Science Society of America J.* 75:389-396.

Ferreira, D.R., C.P. Schulthess, and M.V. Giotto. 2012. An investigation of strong sodium retention mechanisms in nanopore environments using nuclear magnetic resonance spectroscopy. *Environmental Science & Technology* 46:300-306.

Fuller, A.J., S. Shaw, M.B. Ward, S.J. Haigh, J.F.W. Mosselmans, C.L. Peacock, S. Stackhouse, A.J. Dent, D. Trivedi, and I.T. Burke. 2015. Caesium incorporation and retention in illite interlayers. *Applied Clay Science* 108:128-134.

Gaines, G.L., and H.C. Thomas. 1953. Adsorption studies on clay minerals. II. A formulation of the thermodynamics of exchange adsorption. *J. Chemical Physics* 21:714-718.

Glueckauf, E. 1949. Activity coefficients in concentrated solutions containing several electrolytes. *Nature* 163:414-415.

Grandjean, F. 1910. Optical study of the absorption of the heavy vapors by certain zeolites. *Comptes Rendus de l'Académie des Sciences* 149:866-868.

Hauser, E.A. 1953. Colloid science of montmorillonite and bentonites. *Clays and Clay Minerals* 2:439-461.

Helfferrich, F.G. 1962. Ion exchange. McGraw-Hill, NY.

Ishida, H., and T. Agag. 2011. Handbook of benzoxazine resins. Elsevier, Amsterdam.

Kerr, H.W. 1928. The nature of base exchange and soil acidity. *Agronomy J.* 20:309-335.

Kinoshita, N., K. Sueki, K. Sasa, J.-I. Kitagawa, S. Ikarashi, T. Nishimura, Y.-S. Wong, Y. Satou, K. Handa, T. Takahashi, M. Sato, and T. Yamagata. 2011. Assessment of individual radionuclide distributions from the Fukushima nuclear accident covering central-east Japan. *Proceedings of the National Academy of Sciences USA* 108:19526-9529.

Kitagawa, S., Kitaura, and S.-I. Noro. 2004. Functional porous coordination polymers. *Angewandte Chemie International Edition* 43:2334-2375.

Kukut, Manolya, B. Kiskan, and Y. Yagci. 2009. Self-curable benzoxazine functional polybutadienes synthesized by click chemistry. *Designed Monomers & Polymers* 12:167-176.

Langmuir, I. 1916. The constitution and fundamental properties of solids and liquids. *J. Am. Chem. Soc.* 38:2221-2295.

Mähler, J., and I. Persson. 2012. A study of the hydration of the alkali metal ions in aqueous solution. *Inorganic Chemistry* 51:425-438.

Misaelides, P., 2011. Application of natural zeolites in environmental remediation: A short review. *Microporous and Mesoporous Materials* 144:15-18.

Motokawa, R., H. Endo, S. Yokoyama, S. Nishitsuji, T. Kobayashi, S. Suzuki, and T. Yaita. 2014. Collective structural changes in vermiculite clay suspensions induced by cesium ions. *Scientific Reports* 4:6585.

Nakao, A., Y. Thiry, S. Funakawa, and T. Kosaki. 2008. Characterization of the frayed edge site of micaceous minerals in soil clays influenced by different pedogenetic conditions in Japan and northern Thailand. *Soil Science and Plant Nutrition* 54:479-489.

Ohno, Takeshi, Y. Muramatsu, Y. Miura, K. Oda, N. Inagawa, H. Ogawa, A. Yamazaki, C. Toyama, and M. Sato. 2012. Depth profiles of radioactive cesium and iodine released from the Fukushima Daiichi nuclear power plant in different agricultural fields and forests. *Geochemical J.* 46:287-295.

Peng, J.-F., Y.-H. Song, P. Yuan, X.-Y. Cui, and G.-L. Qiu. 2009. The remediation of heavy metals contaminated sediment. *J. Hazardous Materials* 161:633-640.

Ray, S.S., and M. Bousmina. 2005. Poly(butylene Succinate-co-adipate)/montmorillonite nanocomposites: Effect of organic modifier miscibility on structure, properties, and viscoelasticity. *Polymer* 46:12430-12439.

Robinson, B.P. 1962. Ion-exchange Minerals and disposal of radioactive wastes: A survey of literature. U.S. Govt. Print. Off. USGS1616:132

Schulthess, C.P., and D.L. Sparks. 1991. Equilibrium-based modeling of chemical sorption on soils and soil constituents. *Advance in Soil Science.* 16:121-163.

Schulthess, C.P., R.W. Taylor, and D.R. Ferreira. 2011. The nanopore inner sphere enhancement effect on cation adsorption: Sodium and nickel. *Soil Science Society of America J.* 75:378-388.

Smith, D.W. 1977. Ionic hydration enthalpies. *J. Chemical Education* 54:540-542.

Sparks, D.L. 2000. Bioavailability of soil potassium. Pages D38-D53, *In* M.E. Sumner (ed.) *Handbook of soil science*. CRC Press. Boca Raton, FL.

Speight, J.G. 1980. *The chemistry and technology of petroleum*. M. Dekker. New York.

Sposito, G. 1989. The chemistry of soils. Oxford University Press, New. York, NY.

Tanaka, K., Y. Takahashi, A. Sakaguchi, M. Umeo, S. Hayakawa, H. Tanida, T. Saito, and Y. Kanai. 2012. Vertical profiles of iodine-131 and cesium-137 in soils in Fukushima prefecture related to the Fukushima Daiichi nuclear power station accident. *Geochemical J.* 46:73-76.

Tsukada, H., H. Hasegawa, S. Hisamatsu, and S. Yamasaki. 2002. Transfer of ^{137}Cs and stable Cs from paddy soil to polished rice in Aomori, Japan. *J. of Environmental Radioactivity* 59:351-363.

Vanselow, A.P. 1932. Equilibria of the base-exchange reactions of bentonites, permutites, soil colloids, and zeolites. *Soil Science* 33:95-114.

Vermeiren, W., and J.-P. Gilson. 2009. Impact of zeolites on the petroleum and petrochemical industry. *Topics in Catalysis* 52:1131-1161.

Violante, A., V. Cozzolino, L. Perelomov, A.G. Caporale, and M. Pigna. 2010. Mobility and bioavailability of heavy metals and metalloids in soil environments. *J. Soil Science and Plant Nutrition* 10:268-292.

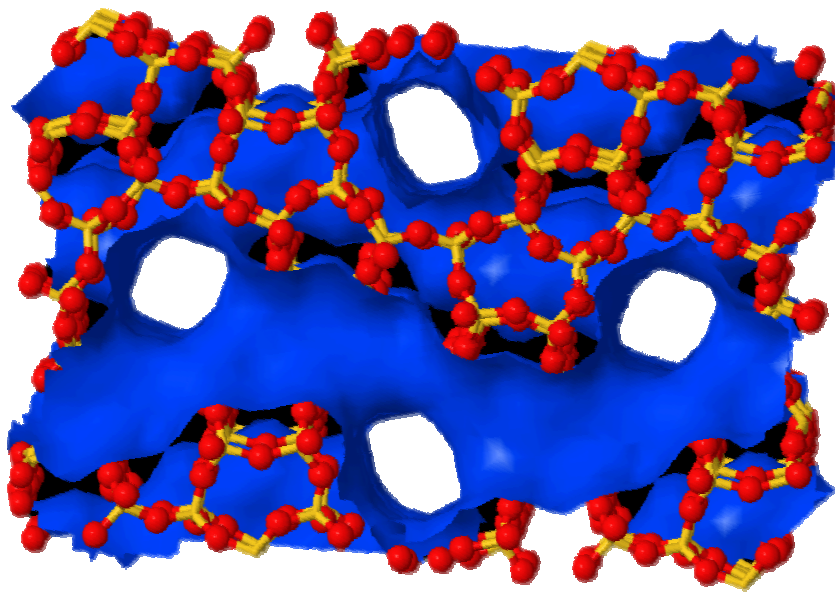
Virta R.L. 2000. Zeolites. U.S. Geological Survey Minerals Yearbook. 85.1-85.4.

Wakeel, A. 2013. Potassium-sodium interactions in soil and plant under saline-sodic conditions. *J. Plant Nutrition and Soil Science Z. Pflanzenernähr. Bodenk.* 176:344-354.

Yasunari, T.J., A. Stohl, R.S. Hayano, J.F. Burkhart, S. Eckhardt, and T. Yasunari. 2011. *Proceedings of the National Academy of Sciences United States* 108:19530-9534.

Chapter 2

Adsorption Selectivity of Alkali Metals on ZSM-5 and Determination of Adsorption Strength by Ion-Exchange Modeling



Abstract

The adsorption of alkali metals (Na^+ , K^+ and Cs^+) on ZSM-5 zeolite with high aluminum content was studied. Adsorption envelopes were created for each of these alkali metals. The adsorption of alkali metals increased with high aluminum content compared with ZSM-5 with low aluminum content. Four adsorption sites were observed from these adsorption envelopes. The adsorption reactions of alkali metals for four adsorption sites were modeled by using simple and net-neutral ion-exchange software. The model predicted the data well and quantified the adsorption strength of each cation by its equilibrium constant ($\text{p}K$). The selectivity for alkali metals was $\text{Cs}^+ > \text{K}^+ > \text{Na}^+$ for inner-sphere complexes formed on *Sites 1* and 2. The adsorption strength of cations ($\text{p}K$) had a strong correlation with their hydration enthalpy ($\Delta H_{\text{hyd}}^\circ$), indicating that the free energy of the adsorption reaction (ΔG°) is greatly influenced by the ion's hydration enthalpy. The selectivity of the cations on ZSM-5 greatly depends on their free energy of hydration. The $\text{p}K$ values of the weaker Na^+ cations increased when in the presence of strongly adsorbing competitive Cs^+ and K^+ cations. These results can be explained in terms of the known solubility of kosmotropes and chaotropes in bulk solutions, which we extrapolate to also apply to the inside pore channels of ZSM-5.

2.1. Introduction

Zeolites are used in many different fields due to their unique properties as an adsorbent. The structural surface area of zeolites with different dimensions of 3D channels reaches several hundred square meters per gram (Breck, 1974). The adsorption of ions can occur on the external surface of the mineral or the interstitial surface of the nanopores channels of about 0.2 to 1 nm diameter running throughout the material. The pore size properties of zeolites have significant effects on adsorption processes. The ions and molecules with diameters larger than the zeolite's pore size cannot enter the pore channels, which is why zeolites are also known as molecular sieves.

The application of natural zeolites has been widely used for the remediation of hazardous contaminants in the environment (Misaelides, 2011). Natural zeolites are effective at efficiently removing or immobilizing the contaminants from industrial waste and nuclear reactor accidents. The use of natural zeolites as a remediation tool was extensively studied in the previous century, and zeolites such as clinoptilolite were already being applied to immobilize radioactive cesium (Ames, 1962). Synthetically modified zeolites with strong adsorption capacities were recently introduced as reactive barriers to clean contaminated water (Bowman, 2003). The application of natural and synthetic zeolites is becoming one of the efficient materials commonly used for environmental remediation (Misaelides, 2011). The extensive success of zeolites as a remediation tool and in industrial applications is mainly attributed to their crucial properties of high ion-exchange selectivity, high surface area, strong adsorption capacity inside the channels, and extensive structural framework of interconnected pore channels (Yilmaz et al., 2012).

Recent research conducted by Schulthess et al. (2011) and Ferreira and Schulthess (2011) has shown that the different sizes of the pore channels of zeolites can have a significant effect on adsorption capacity. They studied the effectiveness in adsorption selectively of three cations (Na^+ , K^+ , and Ca^+) on four types of zeolites differing in pore size dimensions (small, medium and large) as a function of pH. The zeolite with large pores had much lower adsorption values than the other three zeolites for all the cations studied. These results indicated that the chemical adsorption selectively of cations on zeolites is strongly affected by the physical properties of the channels, and this phenomenon is called the nanopore inner-sphere enhancement (NISE) effect. The NISE effect states that the weakly hydrated ions may dehydrate and adsorb strongly onto mineral surfaces via inner-sphere complexes in the constrained nanopore environment. Subsequent research using nuclear magnetic resonance (NMR) confirmed that Na^+ cations, which typically adsorb very weakly via outer-sphere complexes, were adsorbing via a strong inner-sphere mechanism in the small pore channels, such as those found in ZSM-5 and mordenite (Ferreira et al., 2012). The adsorption site for Na^+ cations on the ZSM-5 zeolites are presumably on the aluminum adsorption sites (Breck, 1974).

Constrained environments of nanometer and sub-nanometer dimensions are pervasive in nature, where they exist as channels in a wide range of minerals (nanopores), clays (planer interlayers), and biological cell walls (ion-channels). Our current understanding of the adsorption processes in these constrained environments and the role of the physics of these environments on their chemical reactivity is limited. This study seeks to further our understanding of nanopores in zeolites in the hope that it will

clarify some important physical chemical properties of these rigid channel structures. Rigid channel structures are also easier to study than those that can change their size or shapes, and hopefully can offer useful data and observations for subsequent studies and discussions of more complex constrained environments.

The first objective of this study was to quantify the effect of aluminum content on the adsorption of alkali metals (Na^+ , K^+ and Cs^+). This was pursued by comparing the Na^+ adsorption on an aluminum rich ZSM-5 zeolite with published results of an aluminum poor zeolite (Ferreira and Schulthess, 2011). The second objective was to describe and quantify the reaction mechanism involved in the adsorption of alkali metals. Specifically, the adsorption data were described using an ion-exchange model to obtain the equilibrium constant (K). The $\text{p}K$ values and adsorption strength of cations, with and without multiple ion competition, can elucidate how the hydration energy and ion interactions are influencing the adsorption processes.

2.2. Materials and Methods

The zeolite used was the NH_4 form of ZSM-5 (Zeolyst International, Conshohocken, PA). The description of ZSM-5 is in Table 2-1. This zeolite was converted into an H-form by heating in a ceramic dish as follows: 1 h at 150 °C, 1 h at 300 °C, and finally 3 h at 500 °C. Slurries were prepared by mixing 97 g of ZSM-5 with 1 L of distilled water in a sealed glass container. Pure air free of CO_2 (Ultra Zero Air, Cheshire CT Plant, McCausland, CT) was bubbled through the slurry at 80 mL min^{-1} to remove the CO_2 gas contaminants. The effluent CO_2 gas concentrations leaving the purging chamber were measured using a $\text{CO}_2/\text{H}_2\text{O}$ analyzer (LI-840, LI-COR, and Lincoln, NE) until the slurry was free of CO_2 . Effluent CO_2 (g) levels started at

approximately 600 ppm (1.160 mg L^{-3}) and the purging process took 2 d to complete. The flow rate of the Ultra Zero Air was then lowered to 10 mL min^{-1} to maintain a constant positive pressure and maintain the slurry stock solution free of CO_2 contaminant. The solids concentration was $13.32 \pm 0.1 \text{ mg zeolite mL}^{-1}$ of slurry, which was determined gravimetrically by measuring the weight of solids remaining after oven drying $5 \pm 0.1 \text{ mL}$ of the slurry overnight.

Stock solutions of $0.244 \text{ mol L}^{-1} \text{ NaOH}$, $0.207 \text{ mol L}^{-1} \text{ KOH}$ and $0.7 \text{ mol L}^{-1} \text{ CsOH}$ were prepared for ion-exchange experiments. Oak Ridge centrifuge tubes (50 mL nominal, Thermo Fisher Scientific, Boston, MA) were used to hold the following mixtures. For single ion-exchange reactions, double deionized H_2O , 5 mL of zeolite slurry, variable amounts of $0.25 \text{ mol L}^{-1} \text{ HCl}$ and stock solutions of 2.9 mL of NaOH , 3.4 mL of KOH or 1 mL of CsOH were added to achieve a total volume of 35 mL. The final concentration of each cation was 20 mmol L^{-1} . The pH was adjusted downward using varying amounts of $0.25 \text{ mol L}^{-1} \text{ HCl}$. The same procedure was used for the competitive ion-exchange reactions, but this time two alkaline solutions were added ($\text{NaOH} + \text{KOH}$, or $\text{NaOH} + \text{CsOH}$) for the two-way competitive reactions, or three alkaline solutions were added ($\text{NaOH} + \text{KOH} + \text{CsOH}$) for the three-way competitive reactions. The equilibrium ionic strength of all the experiments ranged from 0.07 to 0.14 mol L^{-1} . The ionic and hydration diameters as well as the hydration enthalpies of the alkali metal cations are shown in Table 2-2.

The mixtures were placed in a hematology mixer and equilibrated for 18 h at 20°C . The mixture was then centrifuged for 10 min at 27000 g to separate the solid and liquid phases. Finally, an aliquot of the supernatant was withdrawn and analyzed by

High Performance Liquid Chromatograph, (HPLC, Prominence, Shimadzu, Kanda, Japan). The HPLC column used was an IC Y-521 styrene divinylbenzene copolymer (Shodex, New York). The column temperature was kept at 40 °C with a flow rate of 1.2 mL min⁻¹ of 4 mmol L⁻¹ nitric acid. Standard solutions of NaCl, KCl and CsCl were used for calibration. The pH was measured with the aid of pHVreader software (version 1.2, distributed by www.alfisol.com) to ensure that proper pH stability was achieved prior to taking the measurements.

Adsorption envelopes were obtained by calculating the amount of each cation adsorbed (Γ) based on the difference of the amount remaining in the liquid subtracted from the input. The model fit curves were optimized using IExFit software (version 1.1, distributed by www.alfisol.com). This software optimizes the pK and the adsorption maxima values for multi-site and multi-competitive models, assuming that only net-neutral pure ion-exchange reactions are occurring.

Table 2-1. Characteristics of ZSM-5 (MFI). Pore dimensions are from zeolite structures database (www.iza-structure.org). The material descriptions of SiO₂/Al₂O₃ ratio and surface area are from Zeolyst International.

Straight Channels, nm	Zigzag Channels, nm	SiO ₂ /Al ₂ O ₃ Ratio	Surface Area, m ² g ⁻¹
0.51×0.55	0.53×0.56	23	425

Table 2-2. Properties of alkali metal cations. Ionic diameters from Mähler and Persson, (2012), hydrated diameter from Gast (1977) and hydration entropy ($-\Delta H^{\circ}_{hyd}$) from Smith (1977).

Cations	Ionic Diameter, nm	Hydrated Diameter, nm	$-\Delta H^{\circ}_{hyd}$, kJ mol ⁻¹
Na ⁺	0.214	0.716	409
K ⁺	0.286	0.662	322
Cs ⁺	0.356	0.658	264

2.3. Results

2.3.1. *Impact of Aluminum Sites on Sodium Adsorption*

The adsorption of Na^+ cations on ZSM-5 differing in silicate and aluminum ratio ($\text{SiO}_2/\text{Al}_2\text{O}_3$) are shown in Figure 2-1. The magnitude of the Na^+ adsorption envelopes on ZSM-5 with a $\text{SiO}_2/\text{Al}_2\text{O}_3$ ratio of 23 was much greater than with a ratio of 80. Both adsorption envelopes increased with increasing pH and the shapes of the adsorption curves were rather similar. However, the difference in adsorption maxima indicated that the $\text{SiO}_2/\text{Al}_2\text{O}_3$ ratio has a great influence on adsorption. The high aluminum content amplified the adsorption capacity of ZSM-5 and showed multiple small inflections in the adsorption envelope.

2.3.2. *Native Concentrations in ZSM-5*

The amount of ions adsorbed is equal to the initial amount present in the mixture minus the amount remaining at equilibrium. The initial concentrations include the amounts added plus the native concentrations present. The native concentrations of ions are easily quantified based on the amount of ions desorbed at low pH or desorbed in the presence of competing ions. No autochthonous (native) concentrations of K^+ or Cs^+ cations were detected at low pH in our ZSM-5 sample. Trace levels of native Na^+ cations, however, were desorbed in the presence of added K^+ or Cs^+ cations (data not shown). The maximum Na^+ desorption observed was 0.21 mmol L^{-1} (equivalent to $0.04 \mu\text{mol m}^{-2}$) at low pH. Accordingly this native Na^+ concentration was added to the total Na^+ input values present in all adsorption experiments. This was similar to the 0.05% Na_2O (w/w) impurity reported by the manufacture, which corresponds to 0.215 mmol

L^{-1} in our experiments (see addendum 1 for calculations). The ZSM-5 zeolite is stable in acid solutions, with only 0.12% dissolving at pH 1.61 (Ferreira and Schulthess, 2011).

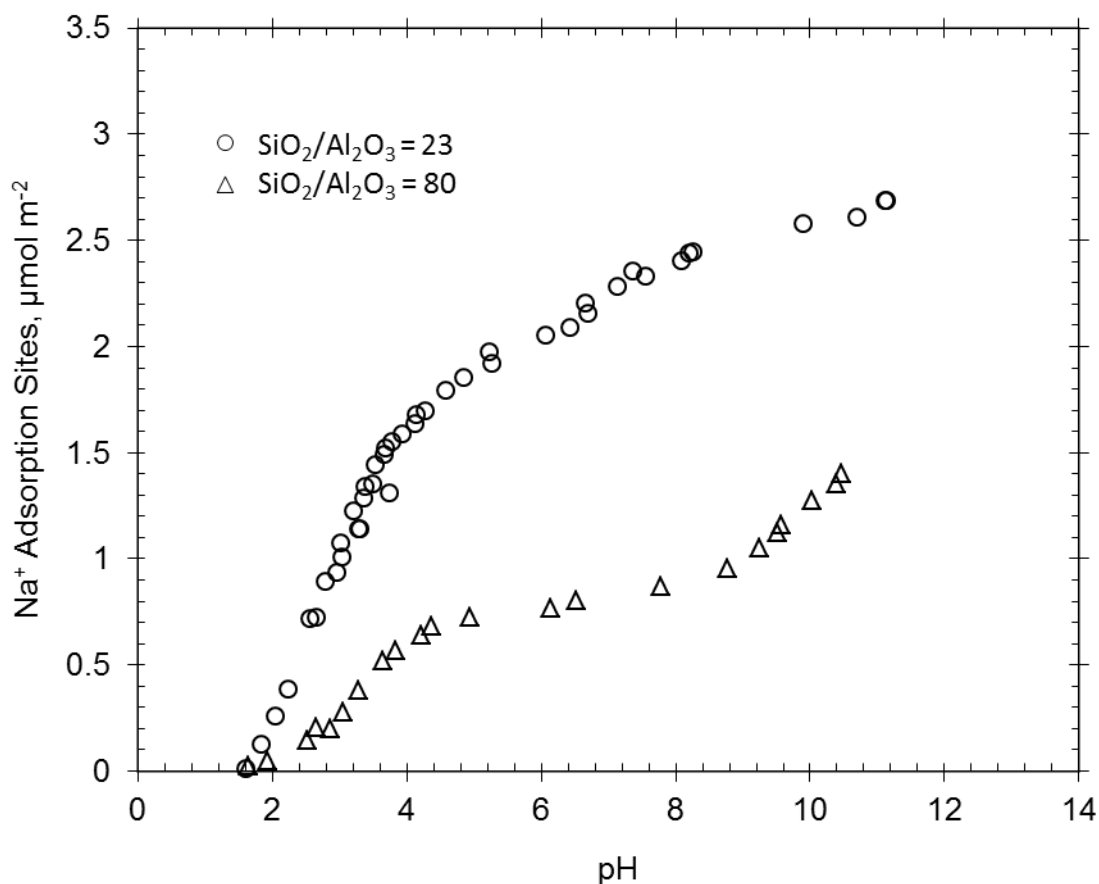


Figure 2-1. Adsorption envelopes of Na^+ on two ZSM-5 zeolites differing in their $\text{SiO}_2/\text{Al}_2\text{O}_3$ ratios. Initial $[\text{Na}^+] \approx 20 \text{ mmol L}^{-1}$. (○) The data points from this study. (□) Data points from Ferreira and Schulthess (2011).

2.3.3. Evaluation of Adsorption Maxima (Γ_{max})

The amount of cations adsorbed on the mineral surfaces depends on the total number of adsorption sites. The cations present in the liquid phase exchange with those on the mineral surface, which will include H^+ cations and result in pH dependent cation adsorption envelopes. When using a multi-site ion-exchange model, the definition of the adsorption maxima is an important criterion. In adsorption envelopes, each adsorption maximum (expressed as Γ_{max} values) and inflection point (expressed as pK values) represent a new surface adsorption reaction. The total adsorption maximum corresponds to the sum of each of the adsorption maxima present on the mineral surface.

The adsorption maximum of each specific adsorption site can be determined from the plateaus in the adsorption envelopes. Some plateaus became more visible by summarizing the cations in competition because the competition of cations amplifies the differences in the adsorption behavior of the various sites present in the mineral. Accordingly, Figure 2-2 describes the total value of the adsorption sites using data for K^+ and Cs^+ cations and cations in competition (Na+Cs and Na+K+Cs). Four adsorption maxima (Γ_{max1} to Γ_{max4}) were observed (Table 2-3).

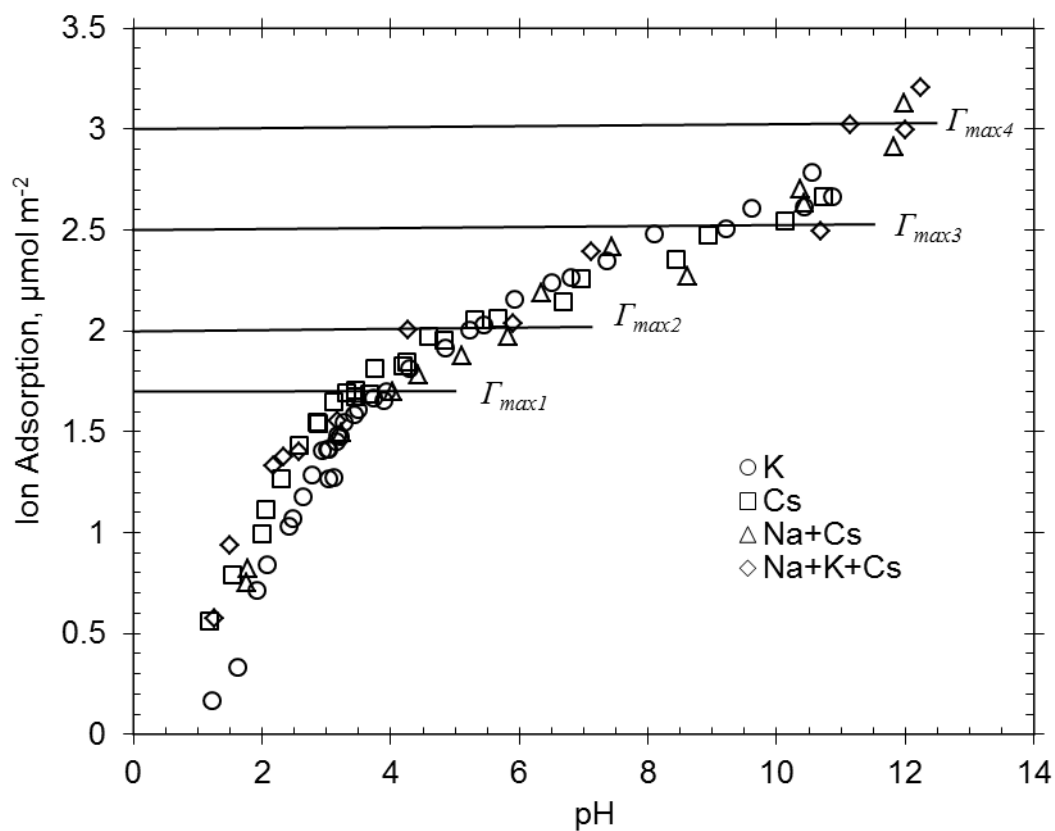


Figure 2-2. Adsorption envelope of various cations to highlight the four adsorption maxima on ZSM-5. Sum of the adsorption values are also shown when multiple cations are present. Initial $[\text{Na}^+]$, $[\text{K}^+]$ and $[\text{Cs}^+] \approx 20 \text{ mmol L}^{-1}$.

Table 2-3. Adsorption maxima (Γ_{max}) and equilibrium constants (pK) of single and competitive ion-exchange reactions (two- and three-way). The correlation coefficient (R^2) shows the goodness-of-fit of the curves in Figures 2-3 and 2-4.

A. Single Reactions

Reactions: $S_jOH + M^+ = S_jOM + H^+$				
Site ID	Γ_{max} , $\mu\text{mol m}^{-2}$	Na ⁺	pK K ⁺	Cs ⁺
1	1.7	1.0	0.5	-0.1
B. Two- and Three-Way Competitive Reactions				
3	0.5	4.9	4.6	4.9
4	0.5	9.0	9.1	8.7
$R^2 =$		0.993	0.977	0.985

Reactions: $S_jOH + M^+ = S_jOM + H^+$				
Site ID	Γ_{max} , $\mu\text{mol m}^{-2}$	Na ⁺	pK K ⁺	Cs ⁺
1	1.7	1.6	0.6	-0.1
2	0.3	3.4	2.8	2.0
3	0.5	5.3	4.6	4.9
4	0.5	9.3	9.1	8.7
$R^2 =$		0.977 (Na w/ K)	0.943 (K w/ Na)	0.907 (Cs w/ Na)
			0.948 (K w/ Na & Cs)	0.936 (Cs w/ Na & K)
		0.902 (Na w/ Cs)		
		0.556 (Na w/ K & Cs)		

2.3.4. Multi-Site Ion-Exchange Adsorption Modeling

Figure 2-3 shows the adsorption envelopes of Na^+ , K^+ and Cs^+ cations along with the multi-site ion-exchange model results using the four site model described in Table 2-3. The curves in Figure 2-3 were generated by using IExFit software to optimize the pK of the four-site ion-exchange model shown in Table 2-3. The correlation coefficients (R^2) measured for the Na^+ , K^+ and Cs^+ cation curves showed high values of 0.977 to 0.993 (Table 2-3A).

The adsorption envelopes showed different adsorption strengths for the reactions at pH 1 to 5.5. The adsorption of Cs^+ cations were always higher than K^+ and Na^+ cations, and the adsorption of K^+ cations were always higher than Na^+ cations. The adsorption maximum in this range corresponds to the reactions in *Sites 1* and 2. However, this trend did not apply to the adsorption envelopes at $\text{pH} > 6$, which correspond to the reactions in *Sites 3* and 4, where all the cations showed similar adsorption patterns. Comparing the pK values between these cations for reactions in *Sites 1* and 2, Cs^+ cations had the lower values (-0.1) followed by K^+ (0.5) and Na^+ (1.0). However, all three cations had similar pK values for reactions in *Sites 3* and 4.

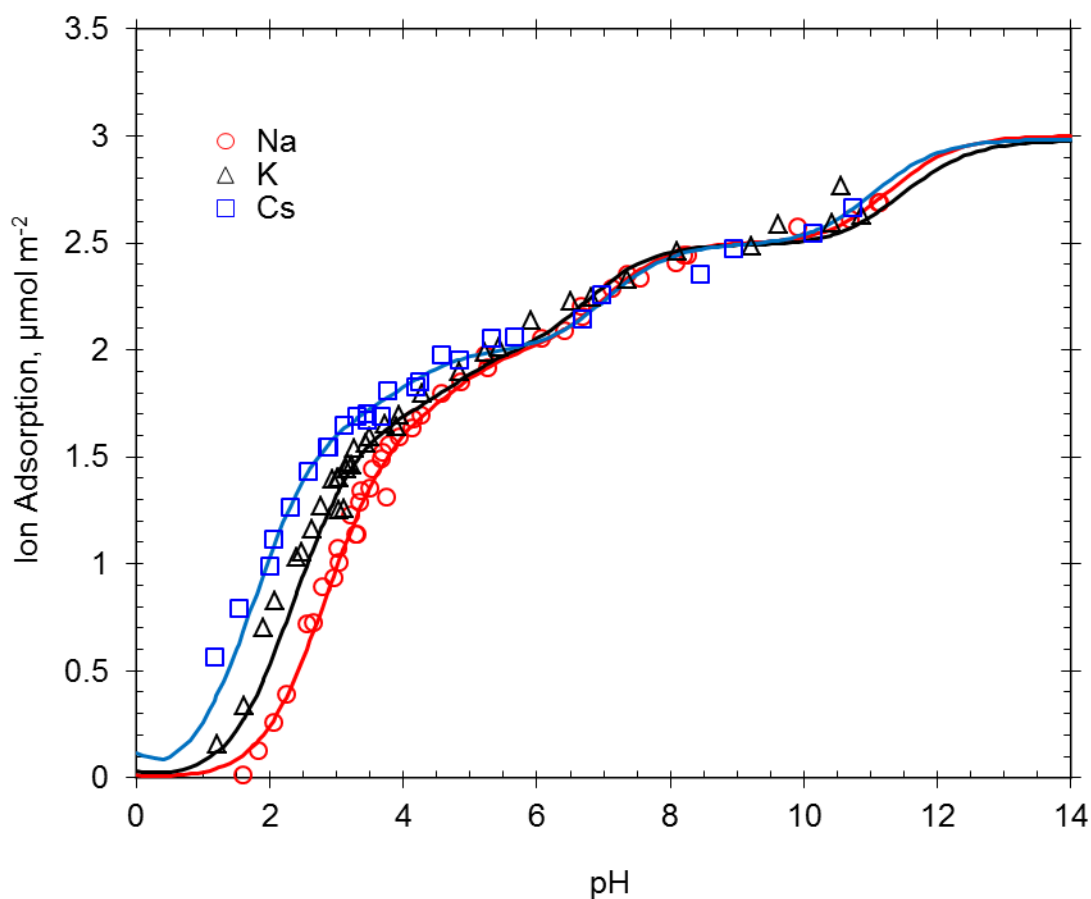


Figure 2-3. Adsorption envelope of Na^+ , K^+ and Cs^+ cations on ZSM-5. Curve fit shown is based on the ion-exchange model described in Table 2-2. Initial $[\text{Na}^+]$, $[\text{K}^+]$ and $[\text{Cs}^+] \approx 20 \text{ mmol L}^{-1}$.

The two-way competition of Na^+ with K^+ and Na^+ with Cs^+ , and the three-way competition of Na^+ with K^+ and Cs^+ were studied. Figure 2-4 shows the adsorption envelopes of these cations in competition with each other along with the results from the multi-site ion-exchange model described in Table 2-3B. The summation of adsorption of each cation in competition ($\text{Na}+\text{K}$, $\text{Na}+\text{Cs}$ and $\text{Na}+\text{K}+\text{Cs}$) is equal to the amount adsorbed by each of the single adsorption envelopes shown in Figure 2-3. Some of the summed cation adsorption envelopes are also shown in Figure 2-2. The adsorption envelopes of Na^+ cations showed a decrease in the presence of K^+ and Cs^+ cations in the

two-way and three-way competition experiments. The adsorption of K^+ cations showed a strong adsorption competition against Na^+ cations in the two-way competition. However, in the three-way competition, K^+ adsorption was weaker in the presence of Cs^+ cations. The adsorption of Cs^+ cations was constantly stronger than Na^+ and K^+ cations in the two-way and three-way competition experiments. In the three-way competition study, these cations showed a strong dependency in adsorption strength following the sequence $Cs^+ > K^+ > Na^+$.

The results of the four-site ion-exchange model used to produce the curves in Figure 2-4 were generated using IExFit software. The curve fit was first attempted using the non-competitive pK values of the single adsorption envelopes. However, the model overpredicted the competitive adsorption data of the Na^+ and K^+ cations. Therefore, the pK values for competitive mixtures were optimized based on two assumptions that will be justified later: (1) each pK value for each cation and each adsorption site is constant if the competing cation is weaker, and (2) the presence of a stronger competitor affects the pK value of the weaker cations. Table 2-3B shows that the pK values of the Na^+ cation from *Sites 1* to *4* had higher values when in the presence of a strong competitor. However, slightly higher values were observed for *Sites 1* and *2* for the K^+ cation in the competing cation assays. None of the Cs^+ pK values changed in the two-way and three-way competitive assays because Cs^+ cation was always the stronger adsorbing cation.

The correlation coefficients (R^2) describing the goodness-of-fit of the curves are shown in Table 2-3B. The correlation coefficient of Na^+ , K^+ and Cs^+ cations in the two-way competition had high values of 0.902 to 0.977, indicating a good curve fit of the experimental data shown in Figure 2-4. The correlation coefficient of the curve fit of the

three-way competition data had high values of 0.948 and 0.936 for K^+ and Cs^+ cations, respectively. However, the model for the three-way competition slightly over predicted the Cs^+ cations at pH 2 to pH 6, and Na^+ cations had a low R^2 value of 0.556. Overall, the R^2 values for all the curves shown in Figures 2-3 and 2-4 were excellent considering the diversity of the experimental conditions involved.

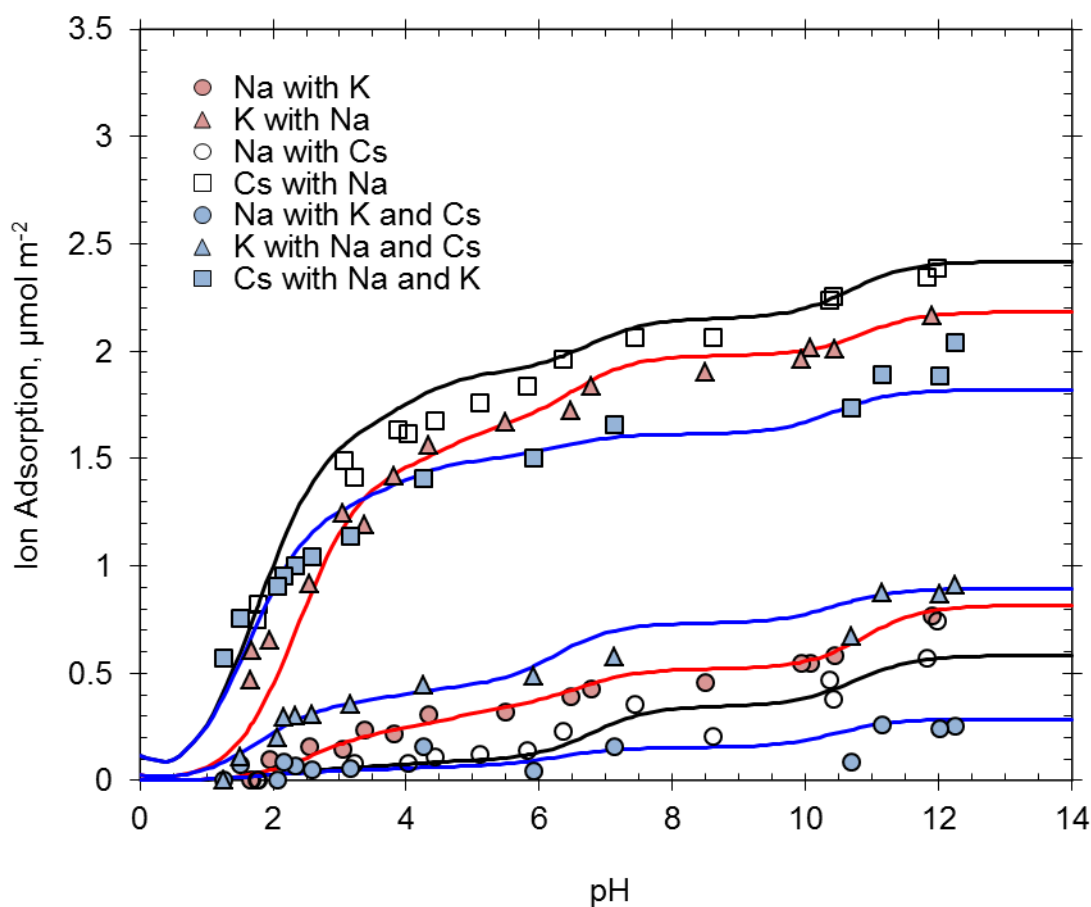


Figure 2-4. Adsorption envelopes of Na^+ , K^+ and Cs^+ cations in two- and three-way competition on ZSM-5. Curve fit shown is based on the ion-exchange model described in Table 2-2. Initial $[Na^+]$, $[K^+]$ and $[Cs^+]$ $\approx 20 \text{ mmol L}^{-1}$.

2.4. Discussion

2.4.1. Impact of Aluminum Sites on Sodium Adsorption

The increase in Na^+ adsorption on ZSM-5 with a high aluminum content ($\text{SiO}_2/\text{Al}_2\text{O}_3 = 23$) shown in Figure 2-1 indicates that the density of aluminum in the framework unit cell directly relates to the total number of adsorption sites. The production of excess negative charges on zeolites by isomorphic substitution of silicate with aluminum is a well-documented phenomenon (Breck, 1974). The number of aluminum atoms in the framework structure can be estimated as follows. The surface area of ZSM-5 is $425 \text{ m}^2 \text{ g}^{-1}$ and the unit cell formula is $(\text{H}, \text{Na})_n[\text{Al}_n\text{Si}_{96-n}\text{O}_{192}]$. The ZSM-5 with a $\text{SiO}_2/\text{Al}_2\text{O}_3$ molar ratio of 23 yields 7.7 aluminum per unit cell ($n = 7.7$) and the formula weight equals $5776.316 \text{ g mol}^{-1}$. Thus, the total number of aluminum sites is $3.13 \text{ } \mu\text{mol m}^{-2}$ ($= n \cdot 10^6 / \text{FW} \cdot \text{SA}$). This number is consistent with the total number of sites of $3 \text{ } \mu\text{mol m}^{-2}$ at pH 12 observed in this study (Figure 2-2 and Table 2-3). Similarly, the estimated total number of aluminum sites of ZSM-5 with a $\text{SiO}_2/\text{Al}_2\text{O}_3$ molar ratio of 80 ($n = 2.3$) was $1.02 \text{ } \mu\text{mol m}^{-2}$, which is close to the data values shown in Figure 2-1. Accordingly, the increase in aluminum adsorption sites amplifies the adsorption envelopes and the majority of the Na^+ cation adsorption is attributed to the aluminum adsorption sites.

2.4.2. Evaluation of Adsorption Maxima (I_{\max})

The presence of four adsorption sites on ZSM-5 described in Figure 2-2 and Table 2-3 agrees with the literature. Using X-ray powder diffraction and crystallography modeling, Olson et al. (2000) identified three Cs^+ cation retention sites on a ZSM-5 with a high aluminum content of 5.8 aluminum per unit cell ($n = 5.8$). One of their Cs^+

retention sites was located in the straight channels, one in the zigzag channels (or sinusoidal channels), and one in the intersections of these two channels. The pH of their dehydrated study was at pH 8 prior to the drying of their material and, as can be seen in Figure 2-2, three adsorption maxima were also observed in the adsorption envelope at pH 8.

Mentzen et al. (2006) identified five dehydrated Cs⁺ cation retention sites on a ZSM-5 with a high aluminum content of 6.9 aluminum per unit cell (n = 6.9). They did not identify the pH equilibrium conditions for their dehydrated Cs⁺ study. However, according to Heo et al. (2009), two of the five Cs⁺ positions reported by Mentzen et al. (2006) were essentially the same as two of the three sites reported by Olson et al. (2000), two others were equivalent to one, and the fifth was new. The article by Heo et al. (2009) arguing a total of four adsorption sites for ZSM-5 agrees with our four-site interpretation shown in Figure 2-2.

The adsorption sites are generated by isomorphic substitution and are generally expressed as aluminum adsorption sites. The Cs⁺ adsorption positions studied by Olson et al. (2000) and Mentzen et al. (2006) were based on aluminum adsorption sites. However, cation adsorption can also occur at a high pH on negatively charged silicate adsorption sites. Olthuis et al. (2005) reported that porous glass silica will form negative surface sites at high pH (pH > 10), where:



Accordingly, the last adsorption maxima observed in Figure 2-2 at pH 11 to 12 could also include silica adsorption sites.

2.4.3. Multi-Site Ion-Exchange Adsorption Modeling

The equilibrium constant (pK) of each adsorption reaction describes the strength of the adsorption reaction. The H^+ cation is competing for adsorption sites in all the adsorption envelopes studied, which results in a pH-dependent adsorption pattern. As the adsorption edge moves further to the left, the pK value of the reaction decreases and reflects the stronger adsorption strength of the target cation relative to the adsorption strength of the competitive H^+ cation. A high pK value indicates a weaker cation adsorption relative to H^+ adsorption. Accordingly, the adsorption strength of each of the cations was strongest for *Sites 1* and *2*, and weakest for *Sites 3* and *4* (Table 2-3). The cation selectivity sequence for the strong adsorption *Sites 1* and *2* was $Cs^+ > K^+ > Na^+$. Conversely, the cation selectivity sequence for the weak adsorption *Sites 3* and *4* were not well defined.

The two primary adsorption mechanisms for cations are electrostatic attraction and chemical adsorption. The electrostatic attraction results in an outer-sphere complex (OS), forms weak adsorption, and is easily replaced by other similarly charged ions. Chemical adsorption results in an inner-sphere complex (IS), forms a strong adsorption bond with the mineral surfaces, and does not easily exchange with other ions. The chemical adsorption mechanisms of the Na^+ cation on ZSM-5 were studied by Ferreira et al. (2012) using Nuclear Magnetic Resonance Spectroscopy (NMR). Their study at pH 7.1 showed that Na^+ adsorbed 84% as IS complexes and 16% as OS complexes. That is, the presence of IS and OS complexes can coexist. The 84% inner-sphere NMR data reported by Ferreira et al. (2012) agrees with our Na^+ adsorption envelope data, where the first surface site with a low pK value corresponds to circa 76% of the total quantity adsorbed (*Site 1*, $\Gamma_{max} = 1.7$ of 2.24 at pH 7.13). If a portion of *Site 2* is also involving an

IS complex, than this estimate increases further. Accordingly, the low pK values (Table 2-3) correspond to strong adsorption mechanisms, and are most likely forming IS complexes. The high pK values correspond to weak adsorption mechanisms, and are most likely forming OS complexes.

The monovalent alkali metals are frequently described as weakly adsorbing OS complexes on mineral surface. However, in small constrained environments, adsorption of cations inside the zeolite pore channels result instead in a significantly strong IS complex. This physical impact on chemical reactions is known as the nanopore inner-sphere enhancement (NISE) effect (Schulthess et al., 2011; Ferreira and Schulthess, 2011). The IS complexes that are formed inside the ZSM-5 at low pH are due to the NISE effect. Schulthess and coworkers proposed that the selectivity of the ions inside the nanopores of zeolites is a function of the free energy of hydration of the ions. Ferreira et al. (2012) confirmed that the heats of exchange of Na^+ and Ca^{2+} cation adsorption inside the ZSM-5 zeolite were consistent with their observed selectivity.

The alkali metals Na^+ , K^+ and Cs^+ in aqueous bulk solutions form a hydration shell consisting of a group of water molecules around them. The hydration of these cations is an exothermic process that releases heat and a decrease in enthalpy ($\Delta H_{\text{hyd}}^\circ$). Highly soluble alkali metals are known to disrupt water structures in bulk solutions to form a single hydration shell (Mähler and Persson, 2012). The hydration shell of these cations affects the hydrogen bonds that make up the bulk structure of water. Water structure making ions (kosmotropes) have small ionic diameter and high charge density, such as Na^+ cations. In the bulk solution, the high charge density of kosmotropes builds a stronger structured network of hydrogen bonds with the surrounding water molecules.

The kosmotropes will decrease the entropy of hydration (ΔS_{hyd}°) and establish a well-organized water structure (Mähler and Persson, 2012). Conversely, water structure breaking ions (chaotropes), such as K^+ and Cs^+ cations with large ionic diameter, have low charge densities that are too weak to build a strong structure around themselves. Thus, chaotropes establish a disorganized water structure.

The diffusion rate of hydrated ionic salts impacts their solubility, with higher solubility observed as the diffusive rate increases. Isha et al. (2003) noted that the diffusion rate of the surrounding water decreased in the presence of kosmotropes, and increased in the presence of chaotropes. Specifically, they observed that the diffusion rate of a dissolved KCl increases slightly as its concentration increases, but it plateaus at around 0.5 mol L^{-1} . Conversely, the diffusion rate of dissolved NaCl continually decreased as its concentration increased. Kosmotropes are attracted to chaotropic water environments and chaotropes are attracted to kosmotropic water environments. Accordingly, kosmotropic-chaotropic salts (where one of the ions making up the salts is a kosmotropes, and the other ion is a chaotropes) are far more soluble than kosmotropic-kosmotropic salts or chaotropic-chaotropic salts. The water structure surrounding kosmotropes becomes larger and even more organized in the presence of chaotropes, while the water structure surrounding chaotropes become even less organized in the presence of kosmotropes (Collins et al., 2004).

The selectivity of the ions in the channels depends on the nature of the surface adsorption sites, the physical d-spacing of the channels, the properties of the solvent, and the properties of the adsorbent. Note that the literature on the solubility of these ions is focused on the kosmotropic and chaotropic cation-anion interactions of salt solvation, but

we postulate here that a similar influence can be posed for kosmotropic cation and chaotropic cation interactions inside the nanopore environments with the negative surface sites acting as surface anions. Ishai et al. (2013) also postulated that the relationship between kosmotropes and chaotropes can influence ion selectivity inside biological K^+ and Na^+ ion-channels. The Na^+ and K^+ ion-channels are highly selective pores in animal and plant cells tissues that produce nerve impulses along neuronal structures. The reported diameter of these channels varies greatly but the minimum diameter of the common ion-channels are 0.3 nm for K^+ channels and 0.62×1.02 nm for Na^+ channels (Laio, 1999). The K^+ channels have a rigid structure, where the K^+ cations partially dehydrate to fit inside the channels (Noskov et al., 2006). Based on molecular dynamics simulations, Noskov et al. (2006) argue that the selectivity for the ion that is transported through the K^+ ion-channels is greatly affected by the channel's size and types of ligands in the binding sites. Noskov et al. (2006) also argue that Na^+ and K^+ adsorption are impacted by the change in the free energy of hydration inside the K^+ ion-channels, but not inside all the other biological ion-channels. The physical dimensions of the nanopore channels of ZSM-5 (Table 2-1) are rigid and are approximately the same size as the biological K^+ ion-channels.

The pK values of Na^+ cations (kosmotropes) in competition with other cations (chaotropes) resulted in higher values compared to non-competing assays (Table 2-3). The shift toward weaker adsorption strength of Na^+ cations in the presence of the stronger competitors indicates that the competitors are affecting the adsorption processes of the Na^+ cation. As noted earlier, the increase in solubility of Na^+ cations in the presence of chaotropes decreases their ability to adsorb, resulting in higher pK values.

In the presence of multiple ions competing for adsorption sites, chaotropes establish a predominantly disorganized water structure in the nanopore aqueous environment. The fully hydrated, large chaotropic Cs^+ and K^+ cations are unable to physically fit inside the pore channels of ZSM-5 (Table 2-1 and 2-2). Instead, they partially dehydrate and establish a new water structure as they enter the channels. Combining the comments made by Ishai et al. (2013) and Collins et al. (2004), the solubility of the kosmotropic Na^+ cations inside the nanopores increased in the presence of the stronger competing cations, but the solubility of the chaotropic Cs^+ or K^+ cations are either not changed or are decreased only slightly in the predominantly disorganized water structure environments. Accordingly, the solubility of the strongly chaotropic Cs^+ cations are probably not influenced by kosmotropes in the nanopore aqueous environments. Interactions between two large chaotropic cations are also very weak (Collins, 1997). Thus, the pK values of Cs^+ cations in the weakly competing environments are not affected (Table 2-3).

Similarly the solubility of the chaotropic K^+ cations are also less influenced by kosmotropes. However, when comparing K^+ with Cs^+ cations, the K^+ cations are less strongly chaotropic. Accordingly, in the presence of equivalent concentrations of kosmotropic Na^+ cations as a competitor (two- and three-way competition), there was a slight increase in the pK values of K^+ cations in *Sites 1* and *2* (Table 2-3).

2.4.4. Impact of Hydration Enthalpy on Equilibrium Constant

The hydration of ions is an exothermic process. The energy released when one mole of an ion in the gaseous state is dissolved and hydrated in water is known as the hydration energy or hydration enthalpy. The hydration enthalpies (ΔH_{hyd}°) of alkali metals are listed in Table 2-2. The adsorption reactions proceed forward when the free energy of the adsorption reaction (ΔG°) is negative, where:

$$\Delta G^\circ = \Delta H^\circ - T\Delta S^\circ \quad [2]$$

and ΔH° = adsorption reaction entropy, ΔS° = adsorption reaction enthalpy, and T = absolute temperature.

This free energy of the adsorption reaction directly relates with the equilibrium constant (pK) where, $\Delta G^\circ = -RT \ln K$. If the hydration enthalpy correlates with the pK values, then the free energy of the adsorption reaction (ΔG°) is greatly influenced by the ion's hydration enthalpy (ΔH_{hyd}°).

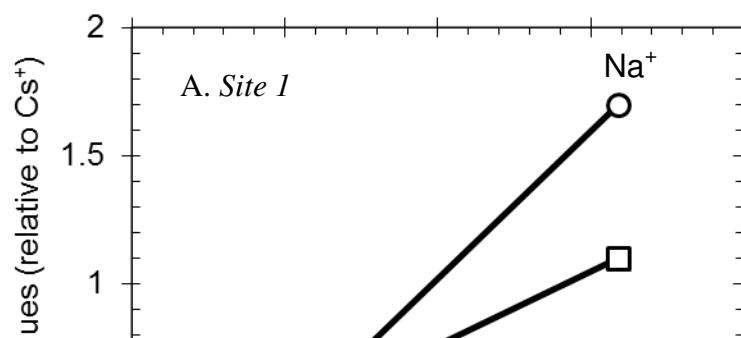
The pK values of Na^+ , K^+ and Cs^+ cations from *Sites 1 to 4* were correlated with their hydration enthalpies (Figure 2-5), and their correlation coefficients (R^2) are shown in Table 2-4. *Site 1* and *2* had very good correlations with high R^2 values, whereas *Site 3* and *4* had low R^2 values except for the competitive reactions in *Site 4* that had high R^2 values of 0.910. *Site 4* was evaluated from Figure 2-2, which assumed that the adsorption reactions ended at pH 12. However, the pH range was not high enough to fully confirm this maximum. Furthermore, the full shape of the adsorption edge is not well defined in this high pH range, which impacts the reliability of the curve fitting procedure. That is, the pK values for *Site 4* are also not well defined in this high pH range.

The competitive reactions showed a better correlation of hydration enthalpy with pK values than the single reactions. This is probably because mixing kosmotropes with

chaotropes will influence their hydration spheres, and as noted earlier, kosmotropes establish a well-organized water structure in the presence of chaotropes (Collins et al., 2004). Thus, the correlation of the pK values to hydration enthalpy (ΔH_{hyd}°) is improved when mixing kosmotropes with chaotropes.

Table 2-4. The correlation coefficient (R^2) obtained from the hydration enthalpy correlated with pK values of Na^+ , K^+ and Cs^+ cations for Sites 1 to 4.

pK	R^2			
	<i>Site 1</i>	<i>Site 2</i>	<i>Site 3</i>	<i>Site 4</i>
Competitive Reactions	1.000	0.962	0.166	0.910
Single Reactions	0.972	0.750	0.013	0.405



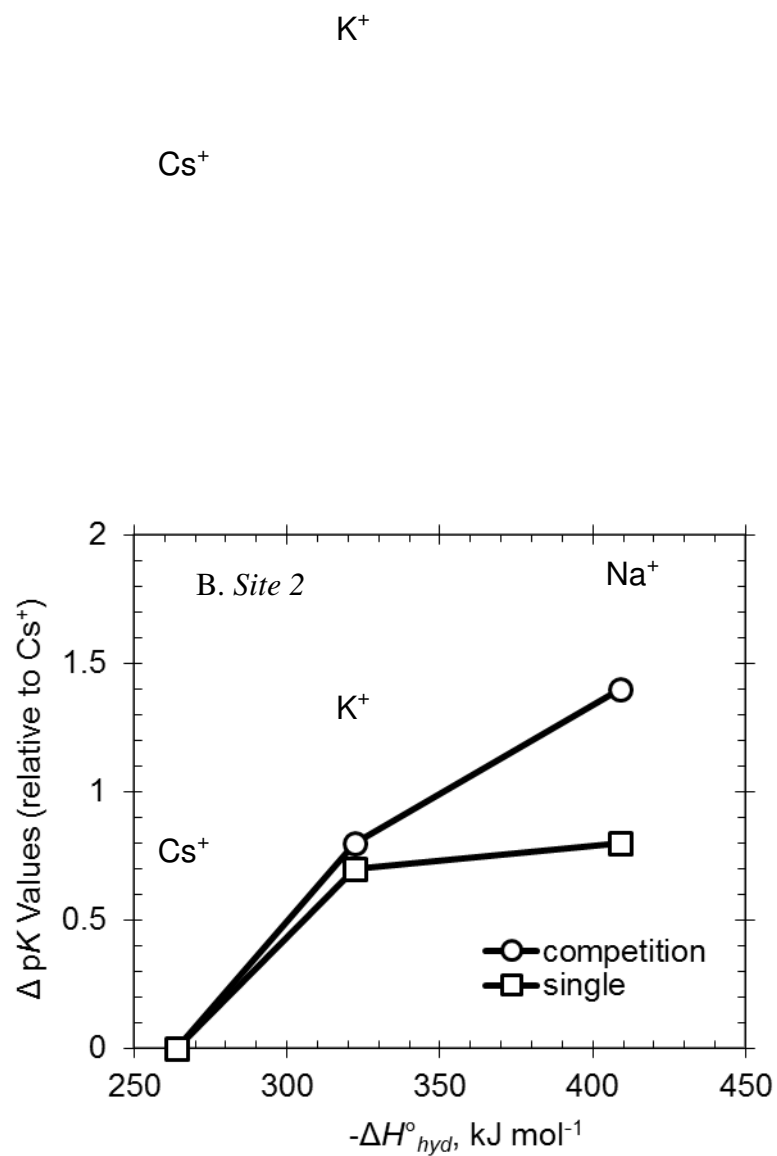


Figure 2-5. Hydration enthalpy versus pK values of Na^+ , K^+ and Cs^+ cations for (A) Site 1 and (B) Site 2.

2.5. Conclusions

The adsorption of alkali metals increased with increasing amount of aluminum per unit cell in the ZSM-5 framework structure. The adsorption sites were mainly controlled by aluminum adsorption sites, but at very high pH the silicate adsorption site may also be involved. Four sites were identified, which agrees with published crystallography studies. The adsorption data was described using a simple, net-neutral, ion-exchange model with four reaction sites. The selectivity for alkali metals was $\text{Cs}^+ > \text{K}^+ > \text{Na}^+$ for IS complexes formed on *Sites 1* and 2. The adsorption strength ($\text{p}K$) of each ion showed a strong correlation with their hydration enthalpy ($\Delta H_{\text{hyd}}^\circ$) indicating that the free energy of the adsorption reaction (ΔG°) is greatly influenced by the ion's hydration enthalpy. The $\text{p}K$ values of the weaker Na^+ cation increased when in the presence of strongly adsorbing competitive Cs^+ and K^+ cations. These results can be explained in terms of the known solubility of kosmotropes and chaotropes in bulk solutions, which we extrapolate to also apply to the inside pore channels of the ZSM-5 zeolite.

References

- Ames, L.L. 1962. Removal of cesium by sorption from aqueous solutions. U.S. Patent No. 30,017,242.
- Bowman, R.S. 2003. Applications of surfactant-modified zeolites to environmental remediation. *Microporous and Mesoporous Materials* 61:43-56.
- Breck, D.W. 1974. Zeolite molecular sieves. Structure, chemistry, and use. Wiley-Interscience, New York, NY.
- Collins, K. 2004. Ions from the Hofmeister series and osmolytes: Effects on proteins in solution and in the crystallization process. *Methods* 34:300-311.
- Collins, K.D. 1997. Charge density-dependent strength of hydration and biological structure. *Biophysical J.* 72:65-76.
- Ferreira, D.R., and C.P. Schulthess. 2011. The nanopore inner sphere enhancement effect on cation adsorption: Sodium, potassium, and calcium. *Soil Science Society of America J.* 75:389-396.
- Ferreira, D.R., C.P. Schulthess, and M.V. Giotto. 2012. An investigation of strong sodium retention mechanisms in nanopore environments using nuclear magnetic resonance spectroscopy. *Environmental Science & Technology* 46:300-306.
- Ferreira, D.R., C.P. Schulthess, and N.J. Kabengi. 2012. Calorimetric evidence in support of the nanopore inner sphere enhancement theory on cation adsorption. *Soil Science Society of America J.* 77:94-99.
- Gast, R.G. 1977. Surface and colloid chemistry. In J.B. Dixon and S.B. Weed (eds), *Minerals in soil environments*. Soil Science Society of America, Madison, WI.
- Heo, N.H., C.W. Kim, H.J. Kwon, G.H. Kim, S.H. Kim, S.B. Hong, and K. Seff. 2009. Detailed determination of the Tl positions in zeolite Tl-ZSM-5. Single-crystal structures of fully dehydrated Tl-ZSM-5 and H-ZSM-5 (MFI, Si/Al = 29). Additional evidence for a nonrandom distribution of framework aluminum. *J. Physical Chemistry C* 113:19937-19956.
- Ishai, P.B., E. Mamontov, J.D. Nickels, and A.P. Sokolov. 2013. Influence of ions on water diffusion—A neutron scattering study. *J. Physical Chemistry B* 117:7724-7728.
- Laio, A., and V. Torre. 1999. Physical origin of selectivity in ionic channels of biological membranes. *Biophysical J.* 76:129-148.
- Mähler, J., and I. Persson. 2012. A study of the hydration of the alkali metal ions in aqueous solution. *Inorg. Chem.* 51:425-438.

Mentzen, B.F., G. Bergeret, H. Emerich, and H.-P. Weber. 2006. Dehydrated and Cs -exchanged MFI zeolites: Location and population of Cs from in situ diffraction data as function of temperature and degree of exchange. *J. Physical Chemistry B* 110:97-106.

Misaelides, P., 2011. Application of natural zeolites in environmental remediation: A short review. *Microporous and Mesoporous Materials* 144:15-18.

Noskov, S.Y., and B. Roux. 2006. Ion selectivity in potassium channels. *Biophysical Chemistry* 124:279-291.

Olson, D.H., N. Khosrovani, A.W. Peters, and B.H. Toby. 2000. Crystal structure of dehydrated CsZSM-5 (5.8Al): Evidence for nonrandom aluminum distribution. *J. Physical Chemistry B* 104:4844-4848.

Olthuis, W., B. Schippers, J. Eijkel, and A.V.D. Berg. 2005. Energy from streaming current and potential. *Sensors and Actuators B: Chemical* 111:385-389.

Schulthess, C.P., R.W. Taylor, and D.R. Ferreira. 2011. The nanopore inner sphere enhancement effect on cation adsorption: Sodium and nickel. *Soil Science Society of America J.* 75:378-388.

Smith, D.W. 1977. Ionic hydration enthalpies. *J. Chemical Education* 54:540-542.

Yilmaz, B., N. Trukhan, and U. Müller. 2012. Industrial outlook on zeolites and metal organic frameworks. *Chinese J. Catalysis* 33:3-10.

Chapter 3

Cation Retention by Montmorillonite in Constrained Environments



Abstract

The retention of cations was studied in constrained and non-constrained environments. Montmorillonite clay minerals were placed in a stainless steel container to limit the expansion of the interlayer and to create a constrained environment. In contrast, montmorillonite clay minerals were suspended in a container for free expansion of the interlayer and to create a non-constrained environment. The Na^+ and Ca^{2+} cations were the dominant native concentrations present in the montmorillonite clay minerals. Cations are likely to form weakly held OS complexes in non-constrained environments, and their adsorption depends greatly on their initial concentrations, ionic hydration diameters, ionic diameters and valences. The adsorption of Na^+ cations increased its adsorption strength in the constrained environments, while the adsorption of the other cations decreased slightly or did not show any changes. This enhanced retention behavior of Na^+ cations may have been due to the nanopore inner-sphere enhancement (NISE) effect.

3.1. Introduction

The physical dimension of zeolites has a significant impact on the adsorption selectivity of cations (Schulthess et al., 2011). Using nuclear magnetic resonance (NMR), Ferreira et al. (2012) confirmed that cations shed their hydration shell to strongly absorb as inner-sphere complexes on the mineral surface when the pore size is small. This phenomenon is called the nanopore inner-sphere enhancement (NISE) effect (Schulthess et al., 2011). The significance of the NISE effect is that the monovalent cations, which are frequently described as weakly adsorbing outer-sphere complexes, destabilize their

hydration sphere and adsorb strongly as inner-sphere complexes inside the small pore channels of zeolites.

Zeolites are hydrated aluminosilicate minerals compositionally similar to clay minerals. The difference in these two minerals is the physical d-spacing inside the framework structures. Zeolites have rigid pore channels that limit the size of the ions that can adsorb on the mineral surfaces through ion-exchange (Helfferich, 1962). In contrast, clay minerals have expansive planar interlayers, with no physical limitations on adsorption selectivity. The hydrated interlayers of montmorillonite can expand in the presence of the dense water molecules associated with ion hydration shells.

Clay minerals in soils are known to immobilize contaminants from industrial waste and nuclear power plants. In the case of the 2012 Fukushima Daiichi Nuclear Power Plant accident in Japan, the emission of radioactive cesium (^{137}Cs , ^{134}Cs) became a serious issue to the surrounding district. Radioactive cesium is highly soluble in water as an alkali metal ion and has a long half-life (30.17 years for ^{137}Cs , 2.0652 years for ^{134}Cs). Radioactive cesium is easily assimilated by living organisms, and is a threat to the food chain and humans (Cremers et al., 1988; Bostick et al., 2002; Tsukada et al., 2002). Spectroscopic studies of radioactive cesium in soils showed a high affinity of this ion to clay minerals (Cha et al., 2006). The radioactive cesium is difficult to remove from the soil once adsorbed by the clay minerals.

Montmorillonite is an aluminosilicate clay mineral commonly found in soils. The structure of montmorillonite consists of two tetrahedral silica sheets surrounding an octahedral alumina sheet. The thickness of each layer is approximately 0.96 nm and the particle diameter is around 300 nm (Ishida, 2011). The interlayer of montmorillonite can

expand extensively though swelling in water, and these interlayers can adsorb ions as outer-sphere complexes (Tao and Chen, 2013). Montmorillonite becomes fully expanded when the interlayer adsorbs hydrated Na^+ cations. The d-spacing of the interlayer can reach 1.7 to 2 nm, whereas the typical interlayer spacing is 0.3 nm to 0.5 nm (Ishida, 2011).

In suspension, the clay mineral expansion is a function of the ion charge density that can enter the interlayer regions to neutralize the charge imbalance in the clay. In packed density environments, the volume is fixed and interlayer expansion is limited by the physical dimensions of the container. In other words, packed environments can be used to control the maximum amount of expansion that a clay mineral is allowed to have. If natural soil environments are similar to packed environments, it follows that the NISE effect observed with rigid channel nanopores in zeolites will also be observed in the interlayer regions of clays. The objective of this exploratory study was to confirm if cation adsorption on montmorillonite is affected by the physical environment of the clay mineral. Specifically, this study seeks to quantify the retention of cations by montmorillonite in constrained and non-constrained environments.

3.2. Materials and Methods

3.2.1. Column Study

The swelling of montmorillonite was controlled by compressing the sand-clay mixture in a stainless-steel container into a fixed volume (Figure 3-1). The total volume of the column was 27.5 cm^3 (0.25 cm inside diameter \times 7 cm tall).

Pure sand was purchased from Thermo Fisher Scientific, Boston, MA. The particle size ranges from 0.150 mm to 0.425 mm (40-100 mesh). The Na-rich

montmorillonite (Swy-2) clay mineral was used as an absorbent (Source Clays Repository, Purdue University, West Lafayette, IN). According to the distributor, the clay has a surface area of $31.82 \pm 0.22 \text{ m}^2 \text{ g}^{-1}$ as determined by BET- N_2 analysis, a $\text{SiO}_2\text{:Al}_2\text{O}_3$ ratio of 3.21:1, and a CEC of 76.4 meq per 100 g.

The column consisted of three layers: (1) sand, (2) sand-clay mixture, and (3) sand. The liquid flow was from bottom to top in the column. At the bottom of the column was a $0.45\text{-}\mu\text{m}$ filter paper (Supor-450, Gelman Sciences). The first layer consisted of 3 g of pure sand above the filter paper. The second layer consisted of a clay-sand mixture, where the amount of clay was always 2 g but the amount of pure sand varied. For the low density experiments, 2 g of clay was mixed homogeneously with 18 g of pure sand, resulting in a 10% clay density. For the high density experiments, 2 g of clay was mixed homogeneously with 2 g of pure sand, resulting in a 50% clay density. The third layer consisted of pure sand, such that the total amount of sand in the column was kept constant at 27 g. This layer contained 5 g of sand for the 10 % clay density, and 21 g of sand for the 50 % clay density. Following this, a $0.45\text{-}\mu\text{m}$ filter paper and a coarse stainless-steel mesh was placed on top. A rubber O-ring was inserted and the dead space in the middle of O-ring was filled with 1 g of pure sand. Note that the 27 g of total sand in the column includes this 1 g of sand. Above this was a $0.2\text{-}\mu\text{m}$ filter paper (Supor-200, Gelman Sciences), followed by another protecting $0.45\text{-}\mu\text{m}$ filter paper on top. Finally, a fine stainless-steel mesh was placed and a stainless-steel plunger was pressed down against the stainless-steel mesh to fix the volume and prevent expansion. The total volume inside the reaction column was $6.55 \text{ mL} \pm 0.16$. Note that high pressure builds up at the bottom of the column when using the higher clay packing density.

Polytetrafluoroethylene (Teflon) tape was used on the threads to achieve a leak-proof container.

Stock solutions of 10 mmol L⁻¹ CsCl, 10 mmol L⁻¹ KCl and 5 mmol L⁻¹ CaCl₂ were prepared for ion-exchange experiments. The sample in the stainless-steel column was equilibrated with 30 mL of these cation containing solutions. Fluid was delivered to the column using a Syringe Pump (KD Scientific Model 410) fitted with an 8 mL stainless-steel syringe (Cole Parmer). The solution was cycled from the bottom to the top of the column 7 mL, with the column effluent flowing back into the original reservoir to create a closed loop. The flow rate was 0.006 mL min⁻¹. This slow flow rate from bottom to top of column removed the entrained air in the column. After at least 5 cycles, the effluent was analyzed for pH and cation concentrations. The pH was 7.6 ± 0.1 for all column experiments. The cation concentrations were analyzed using High Performance Liquid Chromatography (HPLC, Prominence, Shimadzu, Kanda, Japan). The HPLC column used was an IC Y-521 styrene divinylbenzene copolymer (Shodex, New York). The column temperature was kept at 40 °C with a flow rate of 1.2 mL min⁻¹ of 4 mmol L⁻¹ nitric acid. Standard solutions of NaCl, KCl and CsCl were used for calibration. An inductively coupled plasma optical emission spectrometer (ICP-OES, Spectro CROS Vision Argon Plasma Spectrometer, Spectro Analytical, Mahwah, NJ) was used for Ca²⁺ cation analysis. The same procedure was used for the competitive ion-exchange reactions, but this time two cations were present in the initial solutions (CsCl + KCl, or CsCl + CaCl₂).

3.2.2. *Suspension Study*

The montmorillonite clay minerals were suspended without fixing the volume. This allows free-expansion of clay minerals when hydrated. Oak Ridge centrifuge tubes (50 mL nominal, Thermo Fisher Scientific, Boston, MA) were used to contain 2 g of montmorillonite clay minerals plus 30 mL of liquid solutions. The liquid solutions used for the experiments were the same as those used for the column study: 10 mmol L⁻¹ CsCl, 10 mmol L⁻¹ KCl, and 5 mmol L⁻¹ CaCl₂. The mixture was equilibrated in a hematology mixer for 24 h at 20 °C. It was then centrifuged for 20 min at 1000 g to separate the solid and liquid phases and filtered through 0.1-µm filter paper (Supor-100, Gelman Sciences). An aliquot of the supernatant was analyzed for pH and cation concentrations. The final equilibrium pH of the supernatant was 7.6 ± 0.1 for all the experiments. The cation concentrations were analyzed using HPLC. The concentration of Ca²⁺ cations was analyzed by ICP-OES. Similar experiments were also performed with 27 g of sand.

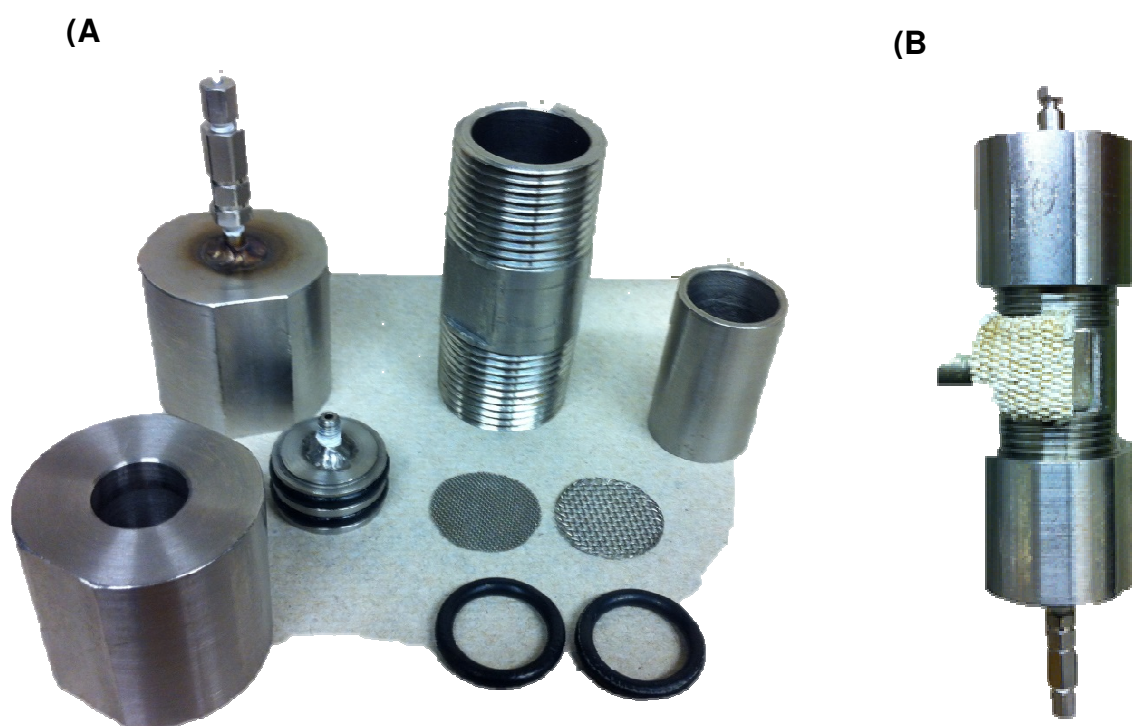


Figure 3-1. (A) The components for construction of the stainless-steel container. (B) Constructed stainless-steel container.

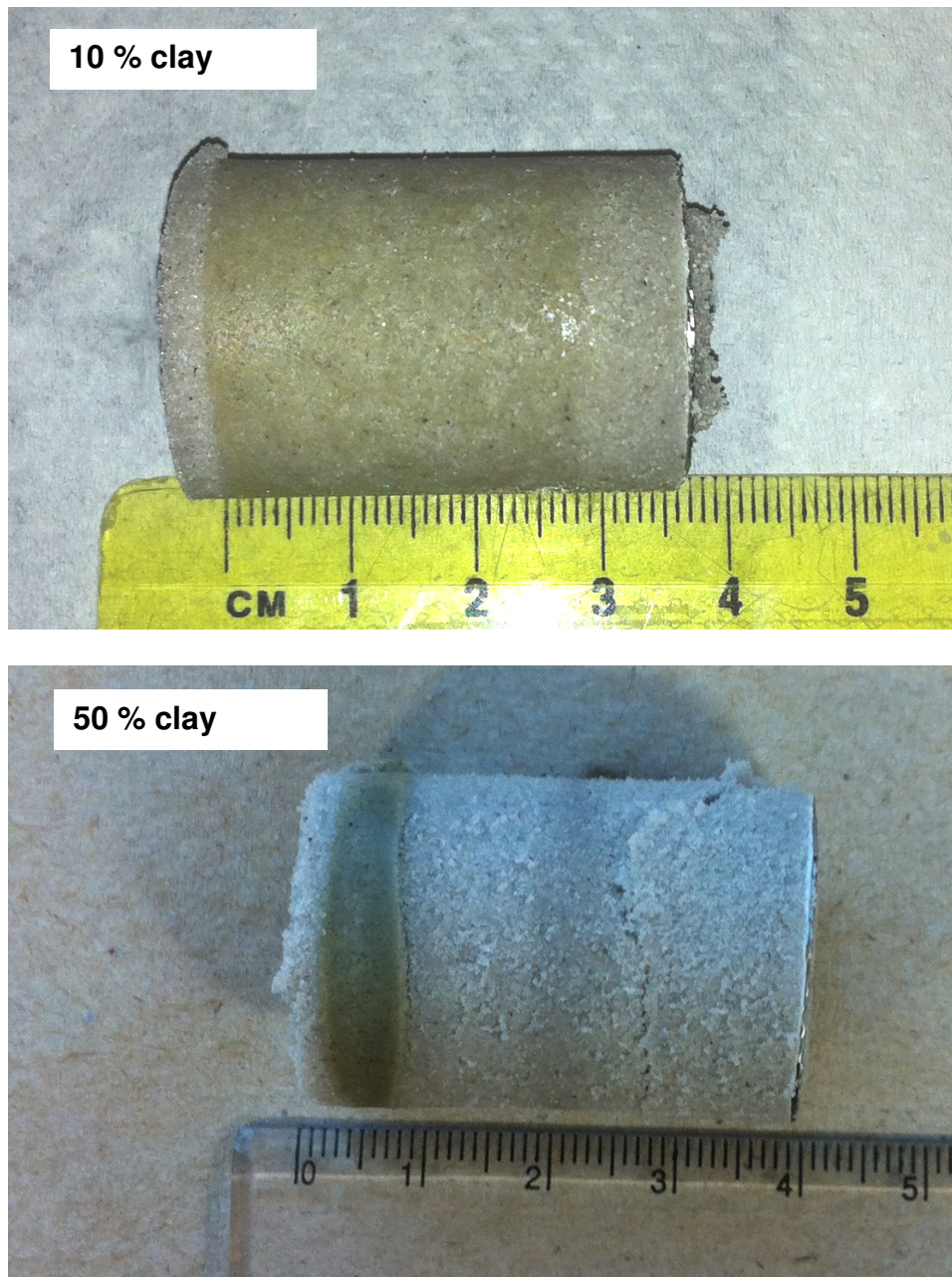


Figure 3-2. The column sand-clay core of 10% and 50% clay densities.

3.3. Results

3.3.1. Native Concentrations in Montmorillonite Clay Minerals

The amount of ions adsorbed is equal to the initial amount present in the mixture minus the amount remaining at equilibrium. The initial concentrations include the amounts added plus the native concentrations present. The native concentrations of ions are easily quantified based on the amount of ions desorbed at low pH. Table 3-1 shows the native concentrations of cations that desorb from 2 g of montmorillonite in 30 mL water at pH 1. No autochthonous (native) concentrations of Cs^+ cations were detected. The native Na^+ and Ca^{2+} cation concentrations were higher than the others and was higher than the Cs^+ cation concentrations that were added. Native concentrations of these cations were also studied for the pure sand using 18 g of sand with 30 mL of $0.25 \text{ mol L}^{-1} \text{ HCl}$, and no impurities were detected.

Table 3-1. Native concentrations of cations in the montmorillonite clay mineral extracted at pH1. Extracted with 2 g of clay by adding 30 mL of $0.25 \text{ mol L}^{-1} \text{ HCl}$. Average of three samples.

Cations	Concentrations, mmol L^{-1}
Na^+	25.2 ± 0.12
Ca^{2+}	18.0 ± 0.02
Mg^{2+}	3.0 ± 0.05
K^+	1.8 ± 0.01
PO_4^{3-} , Mn^{2+} , Zn^{2+} , Fe^{3+} , B^{3+}	trace (≤ 1)

3.3.2. Clay Packing Density

The interlayer of montmorillonite can expand extensively through swelling in water (Figure 3-3a). Inside the column, the expansion of montmorillonite is limited by the fixed total volume of the container. The small clay particles occupy the void space between the sand particles when the sand and clay are mixed together (Figure 3-3b). If the clay content is high, this void space will be completely occupied and the hydrated montmorillonite clay minerals will be less likely to expand their interlayers (Figure 3-3c). The occupancy of clay minerals of the void space was estimated based on the increase in volume of the mixture. The percent of volume increase (Pvi) is defined as follows:

$$Pvi = \frac{V_{sc} - V_s}{V_s} \times 100\% \quad [1]$$

where V_s is the volume of sand and V_{sc} is the volume of the sand-clay mixture. A Pvi value greater than zero indicates that not all the clay particles resided in the available space between the sand particles. For the 10% packing density, the volume of sand was 13 mL and 13.5 mL for the sand-clay mixture, which yields a 4% volume increase. For the 50% packing density, the volume of sand was 1 mL and 3.5 mL for the sand-clay mixture, which is a 250% volume increase. This indicates that the clay particles were already fully occupying the void space between the sand particles at the 10% packing density, but with only 4% above capacity. However, a sand-clay mixture of 50% packing density was much greater than void space capacity. Regardless, both 10% and 50% packing densities lacked space for clay expansion.

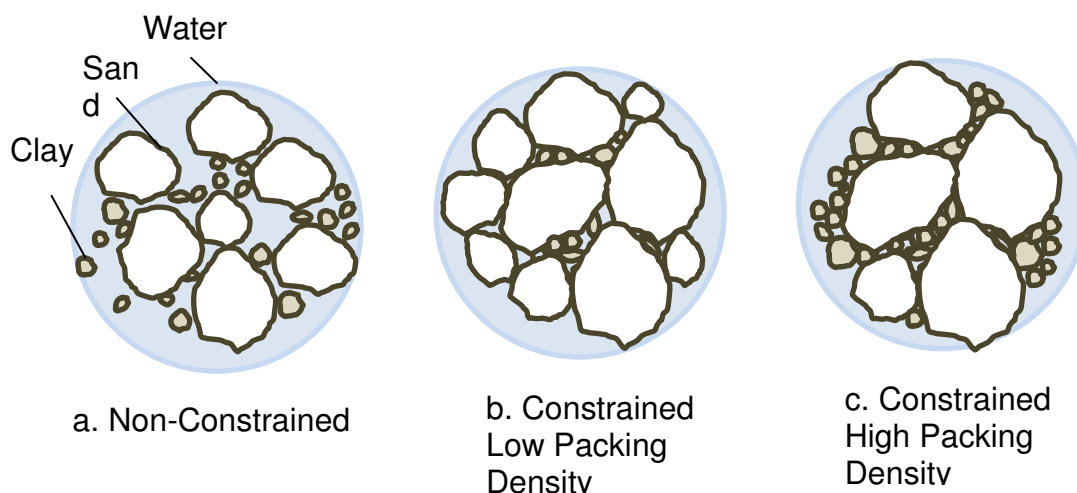


Figure 3-3. Montmorillonite swelling in non-constrained and constrained environments.

3.3.3. Cation Adsorption on Montmorillonite

Figures 3-4 to 3-6 show the adsorption of cations on montmorillonite as a function of packing density. The 0% packing density is the concentration of adsorbed ions when the clay minerals are in suspensions, meaning that the expansion of clay minerals is uninhibited. The 10% and 50% packing densities are the concentration of adsorbed ions when the expansion of clay minerals is controlled by the fixed volume inside the stainless-steel column.

Figure 3-4 shows the adsorption of cations on the montmorillonite clay mineral when 10 mmol L^{-1} of CsCl were added. The Na^+ adsorption increased when the packing density is high, but its adsorption did not change between packing densities of 10% and 50%. The Cs^+ adsorption decreased slightly when the clay was in the column. In contrast, the adsorption of Ca^{2+} , Mg^{2+} and K^+ cations did not change with increasing packing density. The adsorption strength of Na^+ , Cs^+ and Ca^{2+} cations were similar in 0% packing density, whereas the adsorption of Mg^{2+} and K^+ cations were lower.

Figure 3-5 shows the adsorption of cations on the montmorillonite clay mineral when 10 mmol L⁻¹ of CsCl and 10 mmol L⁻¹ of KCl were added. The adsorption of cations had the same trends as those observed in Figure 3-4, where Na⁺ cation concentrations increased and Cs⁺ cation concentrations decreased, and Ca²⁺, Mg²⁺ and K⁺ cation concentrations did not change with increasing packing density. The adsorption of the K⁺ cation increased in increasing concentrations. The adsorption of Cs⁺ and K⁺ cations showed the same adsorption strength at equivalent initial concentrations. The adsorption of K⁺ cations did not show any pattern as a function of packing density.

Figure 3-6 shows the adsorption of cations on the montmorillonite clay mineral when 10 mmol L⁻¹ of CsCl and 5 mmol L⁻¹ of CaCl₂ were added. The Cs⁺ and Na⁺ cations again had the same trends as those observed in Figures 3-4 and 3-5. The interesting behavior was observed with the adsorption of Na⁺ cations. Specifically, the increasing concentrations of the Ca²⁺ cations greatly suppressed the adsorption of Na⁺ cations, and its adsorption was lower than that of the Ca²⁺ cations in 0% packing density. However, this effect was not observed at 10% packing density. Instead, the Na⁺ cations were adsorbing stronger than the Ca²⁺ cations at 10% packing density.

In this study, only single points were collected for each of the experimental assays. Note that the magnitude and shape of all the curves generated were very similar. These results are merely exploratory at the present time.

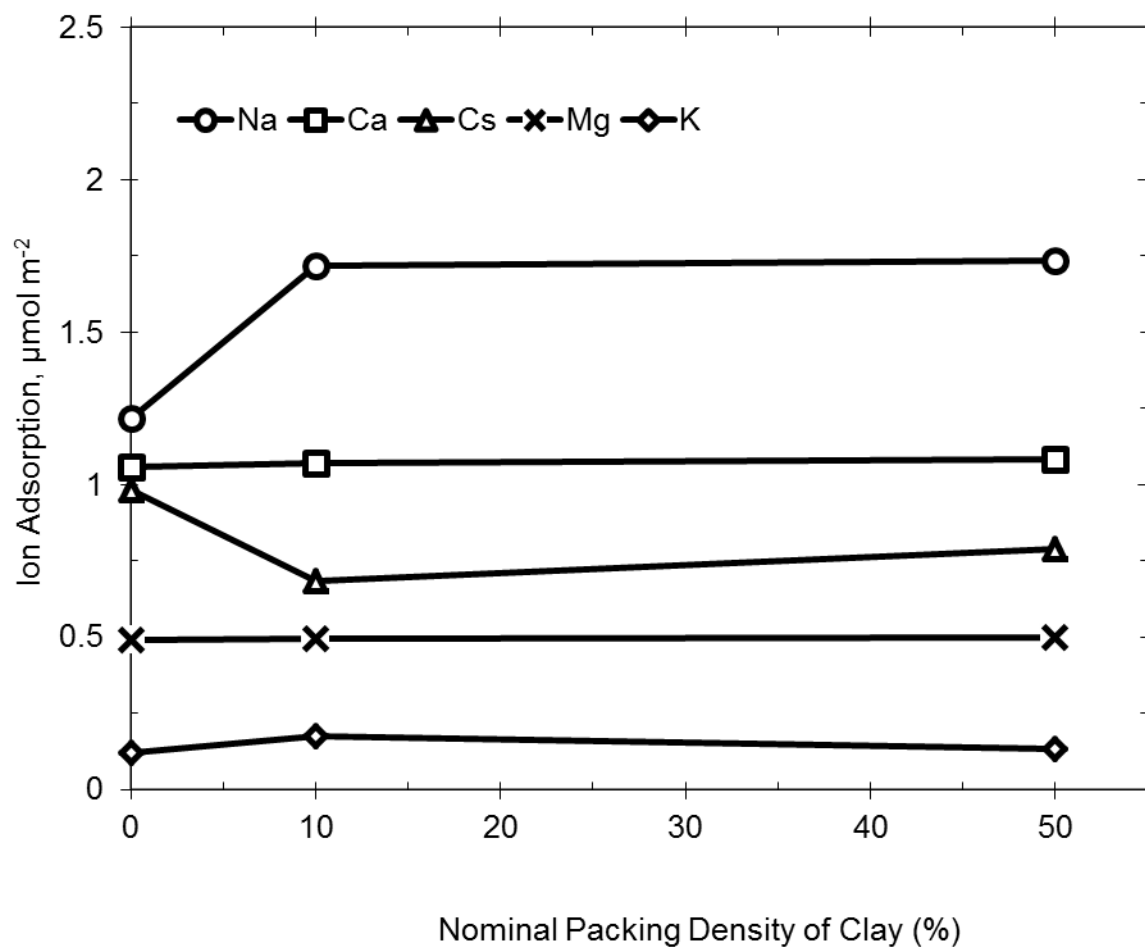


Figure 3-4. Cation adsorption on montmorillonite clay minerals when 10 mmol L^{-1} CsCl were added.

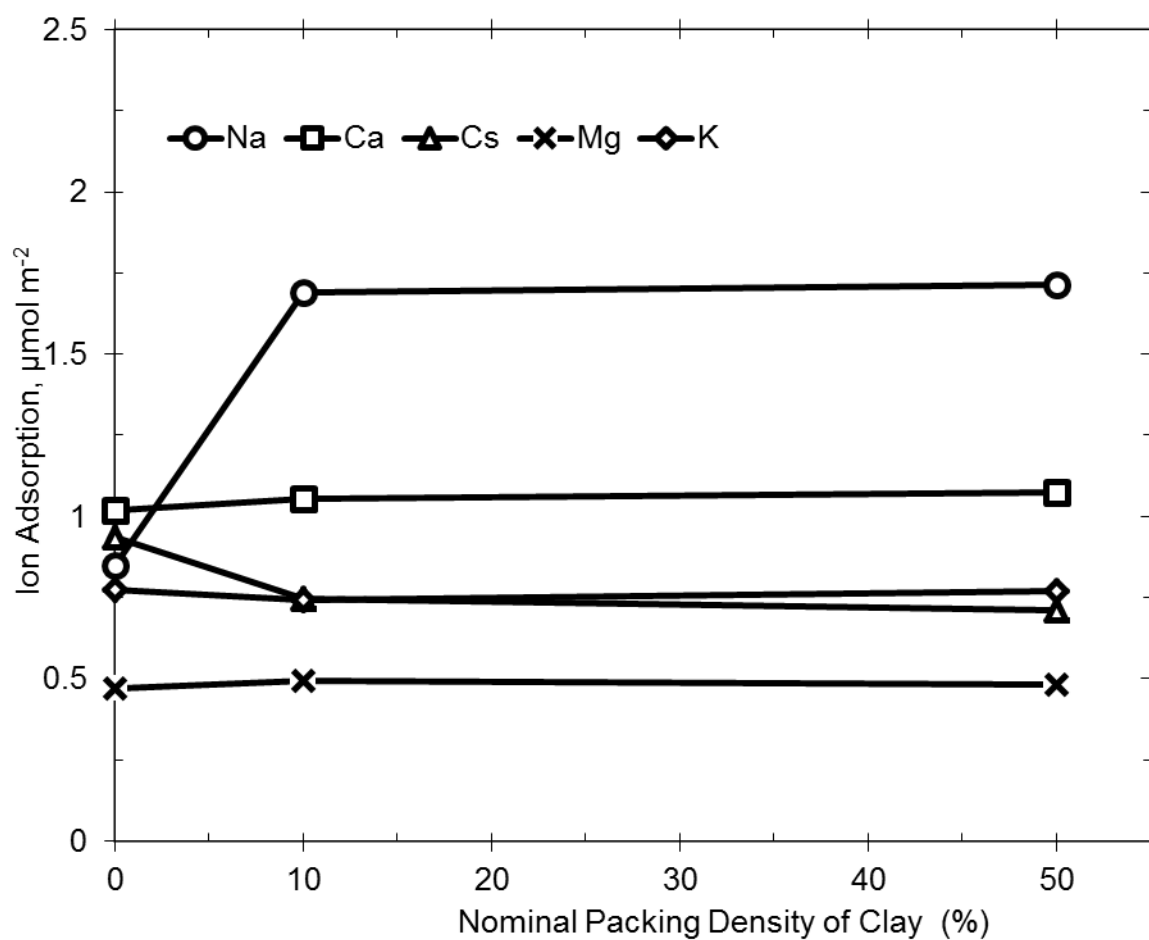


Figure 3-5. Cation adsorption on montmorillonite clay minerals when 10 mmol L⁻¹ CsCl plus 10 mmol L⁻¹ KCl were added.

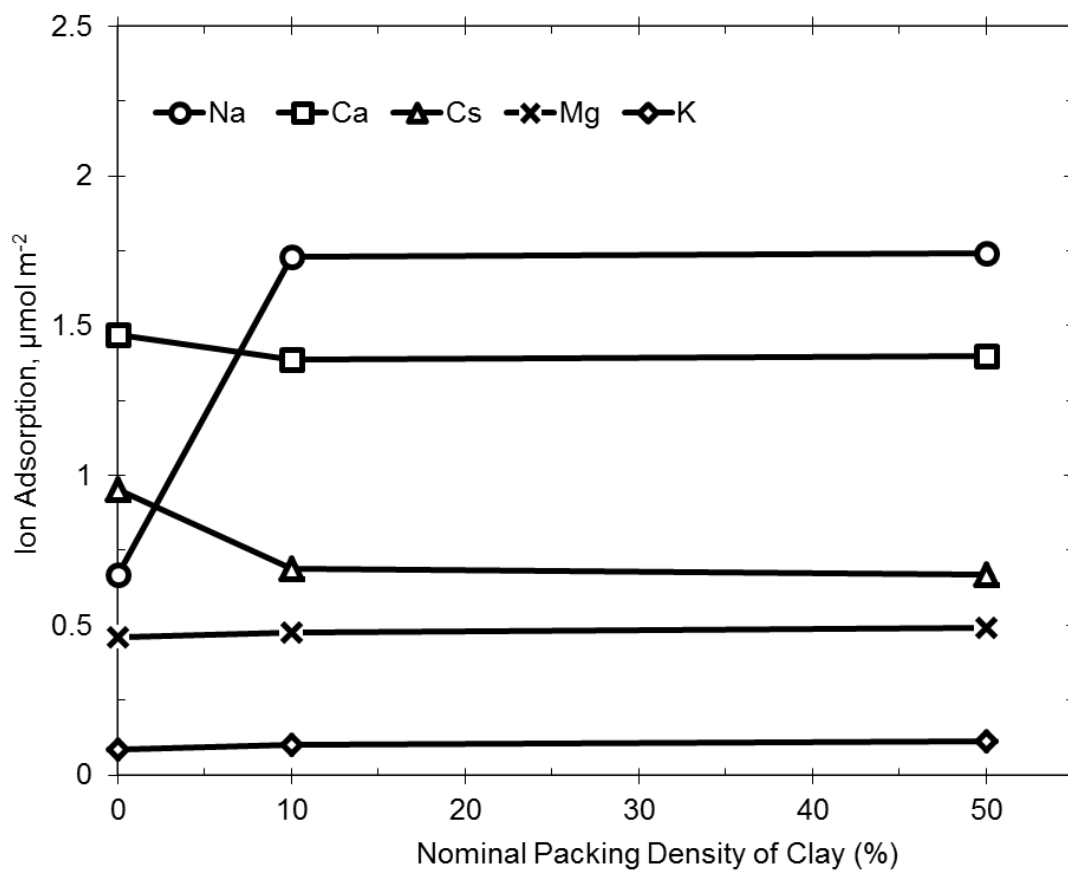


Figure 3-6. Cation adsorption on montmorillonite clay minerals when 10 mmol L⁻¹ CsCl plus 5 mmol L⁻¹ CaCl₂ were added.

3.4. Discussion

3.4.1. Native Concentrations in Montmorillonite Clay Minerals

Montmorillonite is a highly reactive clay mineral with a high exchange capacity (76.4 meq 100 g⁻¹). There is extensive isomorphic substitution within the layers, such as Al³⁺ replaced by Mg²⁺, and Si⁴⁺ replaced by Al³⁺. These substitutions cause an imbalance in the structure and result in charge deficiencies in the particles. The imbalance of the charge is balanced by the hydrated inorganic cations that are retained weakly by electrostatic attraction in the interlayers. Typically the cations retained are exchangeable hydrated Na⁺ or Ca²⁺ cations. This is consistent with the results obtained from the dissolution study (Table 3-1), where the native Na⁺ or Ca²⁺ cation concentrations were high.

3.4.2. Cation Adsorption on Montmorillonite

The adsorption of Ca²⁺, Mg²⁺ and K⁺ cations shown in Figures 3-4 to 3-6 was nearly the same with all the packing densities of 0%, 10% and 50%. This indicated that the adsorption behavior of these cations is similar in the constrained and non-constrained environments. This, in turn, confirms that the liquid flow through the column had good contact with the clay particles and that the column assays had reached equilibrium conditions. However, the adsorption of the Cs⁺ and Na⁺ cations shown Figures 3-4 to 3-6 had different adsorption behaviors between packing densities of 0% and 10%, where the adsorption of the Cs⁺ cations decreased while the Na⁺ cations increased in the constrained environments.

The cations adsorbed in the interlayer are typically known to form weak electrostatic bonds with clay mineral surfaces via outer-sphere complexes (OS) (Tao and Chen, 2013). The Cs⁺ cations also form OS complexes in the hydrated interlayer of montmorillonite (Bostick et al., 2002). According to a molecular dynamics simulation

studied by Tao and Chen (2013), the Cs^+ cations greatly increase the d-spacing of the hydrated montmorillonite clay minerals. The adsorption of Cs^+ cations can expand the hydrated montmorillonite up to 2.2 nm (Tao and Chen, 2013), whereas Na^+ , K^+ and Ca^{2+} cations expand the hydrated montmorillonite up to 1.6 nm (Tao et al., 2010). Their results indicate that the d-spacing in the interlayer is controlled by the physical size of the ions rather than their valences. In Figures 3-4, despite the high native concentrations of Na^+ and Ca^{2+} cations (twice as much as the Cs^+ cations) and the differences in their valences, Na^+ , Cs^+ and Ca^{2+} cations displayed similar adsorption strength for 0% packing density. This is probably because the montmorillonite clay mineral will easily expand its interlayer to accommodate the size of the ions that enter the interlayer, and thus allows those cations to adsorb freely without any physical limitations.

The cations with high initial concentrations (Na^+ , Cs^+ and Ca^{2+}) tend to adsorb more than the cations with low initial concentrations (K^+ , Mg^{2+}). The adsorption of K^+ cations increased in increasing concentrations and showed similar adsorption strength at nearly equivalent initial concentrations with Cs^+ cations (Figure 3-5). This was also observed with the adsorption of alkali metals on ZSM-5 in chapter 2, where all the cations showed similar adsorption patterns at pH 7.6.

The adsorption of Na^+ cations in Figures 3-4 and 3-6 increased with higher packing density. In Figure 3-5, however, weakly adsorbing Na^+ cations were competing with strongly adsorbing Ca^{2+} at nearly equivalent initial concentrations, and this significantly changed their adsorption patterns as a function of packing density. At 0% packing density, the Na^+ and Ca^{2+} cations selectivity was $\text{Na}^+ < \text{Ca}^{2+}$. This is because, at equivalent concentrations, the electrostatic adsorption of the divalent ion is stronger than

the monovalent ion when the interlayer is allowed to expand freely. Conversely, the cation selectivity was $\text{Na}^+ > \text{Ca}^{2+}$ at 10% packing density.

Schulthess et al. (2011) in their study of divalent Ni^{2+} adsorption on a large pore size zeolite, showed that the divalent cations establish a stronger bound on the mineral surfaces when the cations are hydrated, and the selectivity was ($\text{Na}^+ < \text{Ni}^{2+}$). This was because divalent cations have a smaller hydration shell due to their high charge density, and its distance from the surface is closer compared to the monovalent ions with large hydration shells. They also showed that in a medium pore size zeolite, the selectivity was reversed ($\text{Na}^+ > \text{Ni}^{2+}$). Later, Ferreira and Schulthess (2011) also observed this phenomenon with Na^+ and Ca^{2+} cations on zeolites of various pore dimensions. In constrained environments, adsorption of weakly hydrated monovalent cations results in a much stronger IS complex inside the pore channels. The cations with large hydration shells shed their hydration spheres to enter inside the small pore channels and form IS complexes. This physical impact on chemical reactions is known as the nanopore inner-sphere enhancement (NISE) effect.

The increase in Na^+ adsorption at high packing densities (Figures 3-4 to 3-6) may be due to the NISE effect. Inside the column, the expansion of montmorillonite is limited by the available void space of the fixed total volume. The interlayer of hydrated montmorillonite expands and occupies the interparticle spacing between the sand particles. This expansion stops once the entire available void space is occupied. At this point, the clay minerals will be compressed against each other or pressed against the large sand particles (Figure 3-6). This constrained environment should result in rather small interlayer dimensions in the montmorillonite clay minerals.

The Na^+ and Cs^+ adsorption changed from 0% to 10% packing densities, but their adsorption did not change between packing densities of 10% and 50% (Figures 3-4 to 3-6). This result remains unexplained in several aspects. The expansion of hydrated montmorillonite clay mineral is restricted in extremely constrained 50% packing densities compared with 10% packing densities. Thus, the NISE effect was expected to be more pronounced in 50% packing densities. Furthermore, the adsorption of Ca^{2+} , Mg^{2+} and K^+ cations did not change between 0%, 10% and 50% packing densities and only Na^+ and Cs^+ adsorption showed a change between 0% and 10% packing densities. The selectivity of cations on clay minerals remains unexplained and this will be an interesting future topic to study.

The adsorption of Cs^+ cations by clays is often described as retention on frayed-edge sites. A frayed-edge site is a wedge-shaped intermediate zone between non-expanded and expanded layers (Sawhney, 1972; Tamura, 1960). The concept of the frayed edge site was developed from studies of cation adsorption on micaceous minerals, such as illite clay minerals. Micaceous minerals have K^+ cations as structural components of the interlayer, which fix the mineral's d-spacing to a 1.0 nm thickness (Nakao et al., 2008). When the K^+ cations are released from the outer edge through weathering processes, the interlayer will to expand to a 0.4 nm thickness (d-spacing of 1.4 nm). Jackson et al. (1952) conclude that the weathering processes of illite, which breaks down its structure to montmorillonite clay minerals, are due to the production of frayed-edge sites. The Cs^+ cation, which has a low hydration energy, is believed to adsorb preferentially on these frayed-edge sites. This conceptual model of frayed-edge sites has been used extensively to describe the Cs^+ adsorption mechanisms in clay minerals.

However, the occurrence of the frayed edge sites in a very small particle seems unlikely. Pennington (1949) argued that if a single K^+ cation is released from the outer edge opening of the interlayer, the mineral's sheet will rapidly remove the remaining K^+ cations without forming a wedge-shaped intermediate zone. Motalawa et al. (2014) also argue that there is no direct evidence for the existence of frayed-edge sites and that the adsorption studies need to be more closely based on the empirical data.

3.5. Conclusions

The Na^+ and Ca^{2+} cations were the dominant native concentrations present in the montmorillonite clay minerals. Cations are likely to form weakly held OS complexes in the interlayer of suspended montmorillonite clay minerals and the adsorption depends greatly on the ionic size and initial concentrations. The clay packing density greatly affects the adsorption strength of Na^+ cations, where relatively weak adsorption were observed in low packing densities and strong adsorption in high packing densities. This retention behavior of Na^+ cations might be due to the NISE effect. This was an exploratory study on cation adsorption in constrained environments. Recommendations to improve this study are summarized below:

The increase in Na^+ adsorption was observed between the suspended montmorillonite clay minerals and high packing densities inside the column with a fixed volume. In order to confirm or build a theory that the NISE effect applies to these constrained environments, the change in Na^+ adsorption must be confirmed inside the column. The recommendation for further study is to focus on the adsorption behavior of Na^+ cations in extremely low packing densities of around 1 to 5 %. Using EXAFS and

NMR or some other spectroscopies is common method to confirm the complexes formed on the mineral surfaces. This might be the simple way to find out if the Na^+ cations are forming IS complexes inside the column.

The selection of target cations is very important. From Figures 3-4 to 3-6, there were three factors controlling the adsorption in suspended montmorillonite: initial concentrations, ionic charge (monovalent or divalent) and ionic size of cations. The cations with high initial concentrations (Na^+ , Cs^+ and Ca^{2+}) tend to adsorb more than cations with low initial concentrations (K^+ , Mg^{2+}). In general, a divalent cation increases its adsorption because the divalent cation has a smaller hydration shell due to its high charge density. Its distance from the surface is also closer compared to the monovalent ions with large hydration shells. Figure 3-5 shows weakly adsorbing Na^+ cations and strongly adsorbing Ca^{2+} cations in approximately equivalent concentration at 0% packing density. The ionic size greatly influences the distance inside the interlayer of clay minerals. For example, the concentration of Cs^+ cations was half the concentrations of Na^+ and Ca^{2+} cations, but yet the adsorption of Cs^+ , Na^+ and Ca^{2+} cations were more or less similar to each other (Figures 3-4 and 3-5). Accordingly, to amplify the change in Na^+ adsorption between constrained and non-constrained environments, cations with high ionic charge densities and the same or larger ionic sizes are probably good choices.

This study was exploratory but we observed a strong suggestion that the Na^+ cation is adsorbed strongly in constrained environments. The expansion of soils in the environment is also limited by the fixed volume. Future studies might clarify the retention behavior of cations in the natural clay-rich soil environments with high concentrations of Na^+ cations, known as sodic soils.

References

Bostick, B.C., M.A. Vairavamurthy, K.G. Karthikeyan, and J. Chorover. 2002. Cesium adsorption on clay minerals: An EXAFS spectroscopic investigation. *Environ. Sci. Technol.* 36:2670-2676.

Cha, H.J., M.-J. Kang, G.H. Chung, and G.S. Choi. 2006. Accumulation of ^{137}Cs in soils on different bedrock geology and textures. *J. of Radioanalytical and Nuclear Chemistry* 267:349-355.

Ferreira, D.R., and C.P. Schulthess. 2011. The nanopore inner sphere enhancement effect on cation adsorption: sodium, potassium, and calcium. *Soil Science Society of America J.* 75:389-396.

Ferreira, D.R., C.P. Schulthess, and M.V. Giotto. 2012. An investigation of strong sodium retention mechanisms in nanopore environments using nuclear magnetic resonance spectroscopy. *Environmental Science & Technology* 46:300-306.

Ishida, H., and T. Agag. 2011. *Handbook of benzoxazine resins*. Elsevier, Amsterdam.

Jackson, M.L., Y. Hseun, R.B. Corey, E.J. Evans, R.C.V. Heuvel, 1952. Weathering sequence of clay-size minerals in soils and sediments: II. Chemical weathering of layer silicates. *Soil Science Society of America J.* 16:3-6.

Pennington, R.P. 1949. Further studies on glycerol solvation of montmorillonite, and segregation of mineral series for mineralogical analysis of soil clays by X-ray diffraction, exchange capacity, and potassium content criteria. Ph.D. Dissertation, Univ. of Wisconsin.

Sawhney, B.L. 1972. Selective sorption and fixation of cations by clay minerals. *Clays Clay Minerals* 20:93–100.

Schulthess, C.P., R.W. Taylor, and D.R. Ferreira. 2011. The nanopore inner sphere enhancement effect on cation adsorption: Sodium and nickel. *Soil Science Society of America J.* 75:378-388.

Tao, L., and Y. Chen. 2013. A molecular dynamics study of the swelling patterns of Na/Cs-montmorillonite and the hydration of interlayer cations. *Chinese Physics B* 22:027103.

Tao, L., T. Xiao-Feng, Z. Yu, and G. Tao. Swelling of K^+ , Na^+ and Ca^{2+} -montmorillonite and hydration of interlayer cations: A molecular dynamics simulation. 2010. *Chinese Physics B* 19:109101.

Addendum 1

Additional Supporting Data

Additional Supporting Data for Chapter 2

Figure 1. This figure shows the native sodium desorption from ZSM-5 at low pH and in the presence of competing Cs^+ and K^+ ions ($\text{SiO}_2/\text{Al}_2\text{O}_3=23$). In chapter 2, the initial input of Na^+ concentrations were determined from this figure. The total native concentrations were $0.232 \text{ mmol L}^{-1}$.

Calculations of Native Concentrations (page 31)

Na_2O 0.05 % (Impurity in ZSM-5)

$\text{Na}/\text{Na}_2\text{O} = (23 \times 2 \text{ g mol Na} / 62 \text{ g mol Na}_2\text{O}) \times (0.0005 \text{ g Na}_2\text{O} / \text{g ZSM}) = 0.000370968 \text{ g Na/g ZSM}$.

$(0.000370968 \text{ g Na/g ZSM}) \times (0.46625 \text{ g ZSM} / 35 \text{ mL sample}) \times (1 \text{ mmol Na} / 23 \text{ mg}) \times (1000 \text{ mg/g}) \times (1000 \text{ mL/L}) = 0.215 \text{ mmol L}^{-1}$

Figure 2. This figure shows the ion-exchange curve fit of Na^+ adsorption on ZSM-5 differing in $\text{SiO}_2/\text{Al}_2\text{O}_3$ ratio. The data points of Na adsorption on ZSM-5 with $\text{SiO}_2/\text{Al}_2\text{O}_3=23$ ratio from chapter 2 and data points from Na^+ adsorption on ZSM-5 with $\text{SiO}_2/\text{Al}_2\text{O}_3=80$ from the study conducted by Ferreira and Schulthess (2011). This purpose was to model the adsorption envelope of Na^+ ads on a ZSM-5 with different $\text{SiO}_2/\text{Al}_2\text{O}_3$ ratio ($\text{SiO}_2/\text{Al}_2\text{O}_3=23$ and $\text{SiO}_2/\text{Al}_2\text{O}_3=80$) by using the same pK values. Ionic strength is not included.

Figure 3. This figure shows the ion-exchange curve fit of Na^+ adsorption on ZSM-5 differing in $\text{SiO}_2/\text{Al}_2\text{O}_3$ ratio. The data points of Na adsorption on ZSM-5 with $\text{SiO}_2/\text{Al}_2\text{O}_3=23$ ratio is from chapter 2 and data points from Na^+ adsorption on ZSM-5 with $\text{SiO}_2/\text{Al}_2\text{O}_3=80$ is from the study conducted by Ferreira and Schulthess (2011). The adsorption envelope of Na^+ ads on ZSM-5 with $\text{SiO}_2/\text{Al}_2\text{O}_3=23$ was model using the pK values from chapter 2 and ZSM-5 with $\text{SiO}_2/\text{Al}_2\text{O}_3=80$ was modeled by changing the pK values and adsorption maxima of the Na adsorption on ZSM-5 with $\text{SiO}_2/\text{Al}_2\text{O}_3=23$. Ionic strength is not included.

Table 1. pK values and adsorption maxima in Figure 2.

Table 2. pK values and adsorption maxima in Figure 3.

Additional Supporting Data for Chapter 3

Figure 4. This figure shows the adsorption of cations on the montmorillonite clay minerals in the reaction column with 10%, 30% and 50% packing density. The sand-clay mixture was created by adding 1g of clay with different variation of sand. Liquid solution with 30 g of 10 mmol L^{-1} CsCl were cycled at least 6 times to equilibrate the system.

Table 3. This table shows the native concentrations in montmorillonite clay minerals.

Other Additional Data

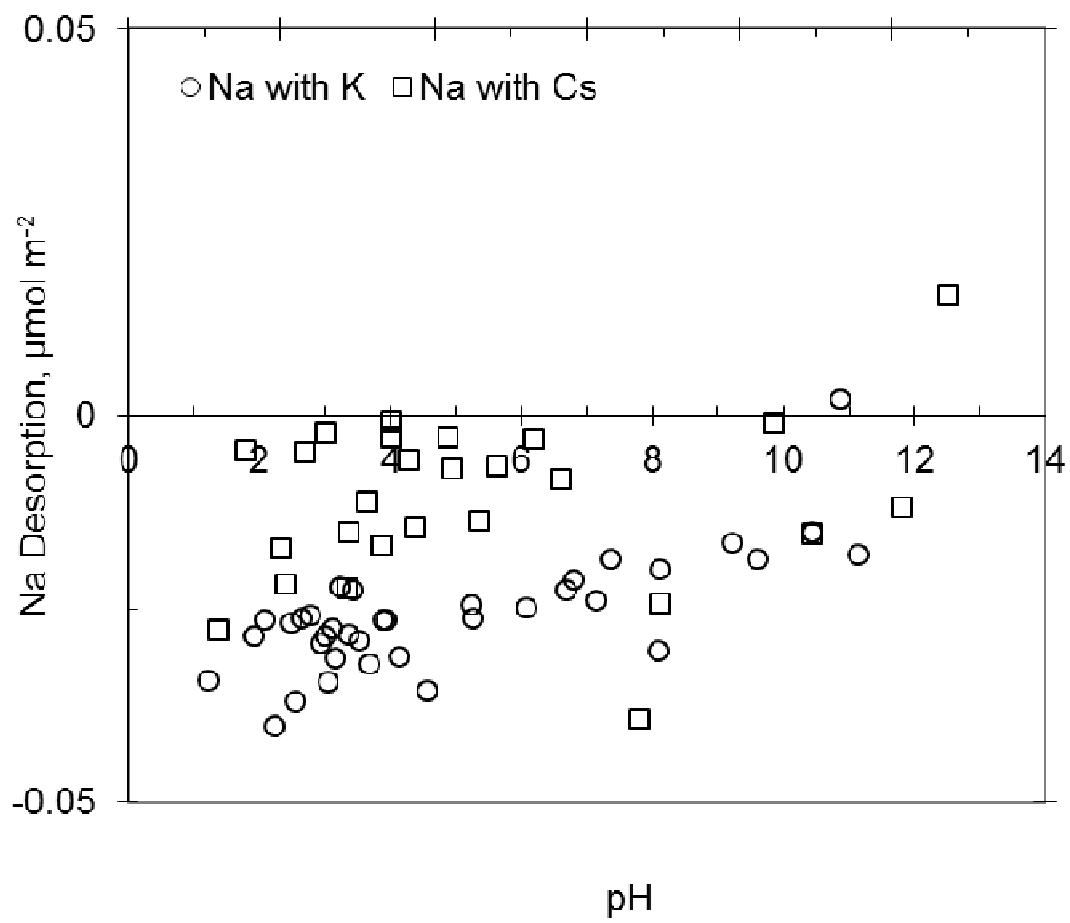
Figure 5. This figure shows the adsorption selenite anions (SeO_3^{2-}) and chloride (Cl^-) on Ferrierite (FER). These anions existed in the same liquid solutions.

Figure 6. This figure shows the adsorption chloride anions (Cl^-) on Ferrierite (FER) in the presence of selenate anions (SeO_4^{2-}).

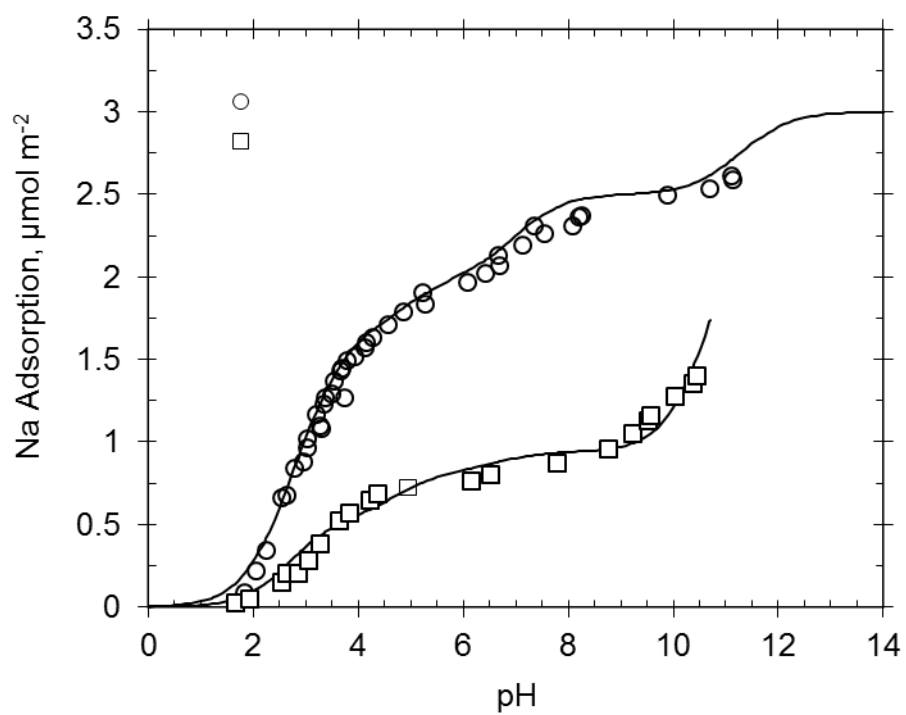
Figure 7. This figure shows the adsorption chloride anions (Cl^-) on Zeolite Y (FAU) in the presence of selenite anions (SeO_3^{2-}).

Figure 8. This figure shows the adsorption chloride anions (Cl^-) on Zeolite Y (FAU) in the presence of selenate anions (SeO_4^{2-}).

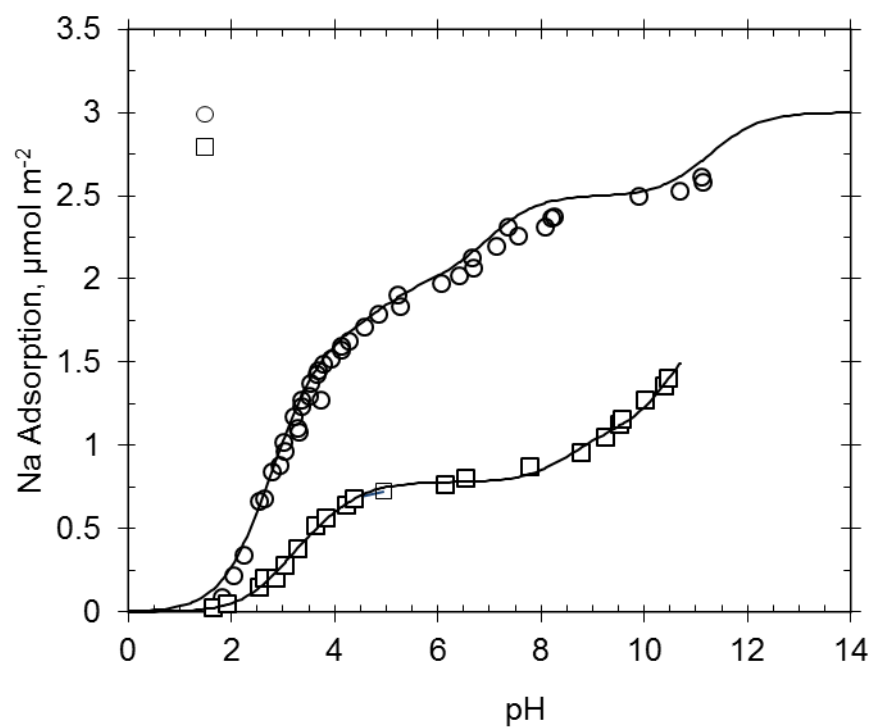
The Figures from 2a to 6b showed the trace levels of anion adsorption occurring inside the zeolites pore channels. These Figures 3 to 6 indicates that anion adsorption does not necessarily occur inside the zeolite pore channels.



≈

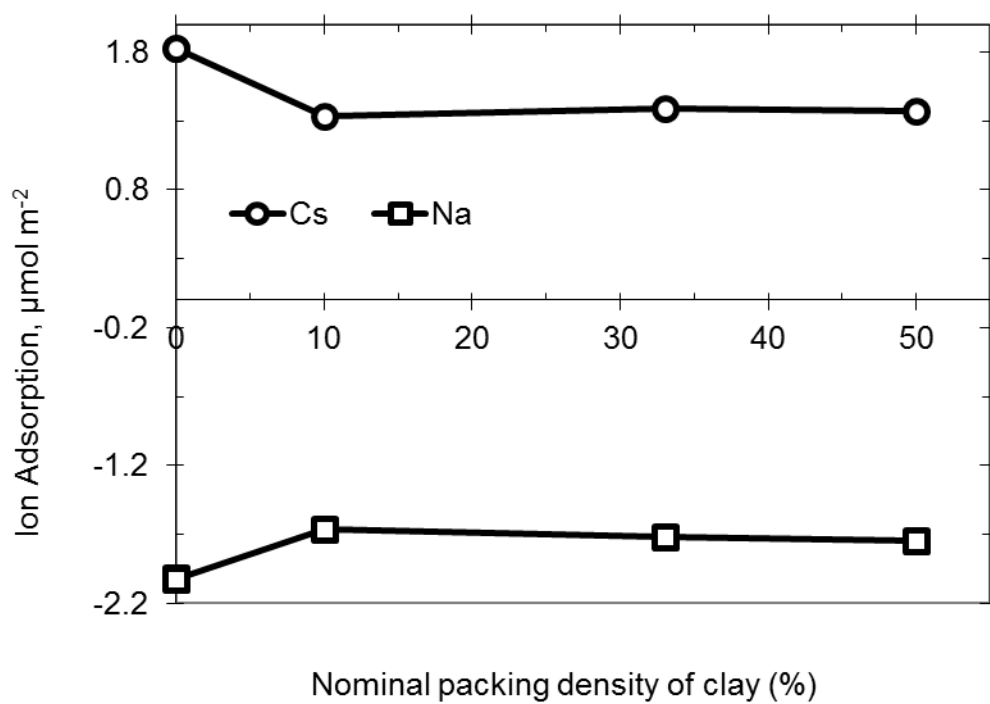


Γ_{max}		
Γ_{max}		
SiO ₂ /Al ₂ O ₃ =23		
Site ID	Γ_{max} (μmol m ⁻²)	pK
1	1.7	1
2	0.3	3
3	0.5	4.9
4	0.5	9
R ² =		0.993
SiO ₂ /Al ₂ O ₃ =80		
Site ID	Γ_{max} (μmol m ⁻²)	pK
1	0.54	1
2	0.28	3
3	0.12	4.9
4	1.86	9
R ² =		0.971

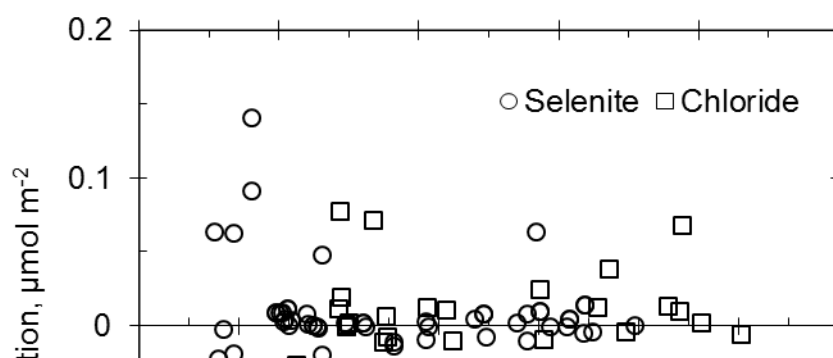


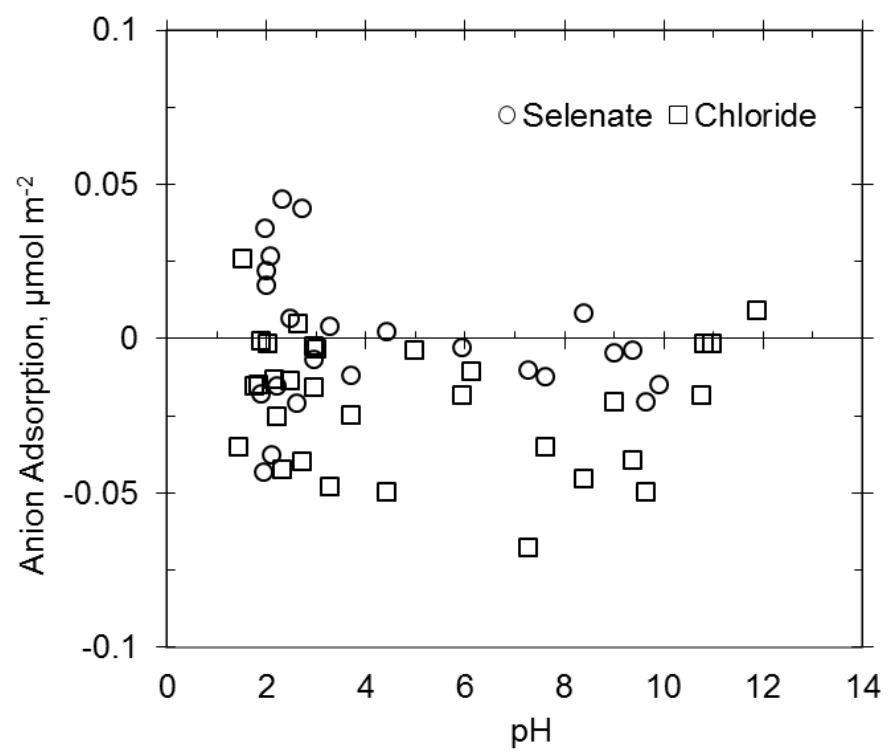
$$\Gamma_{max}$$

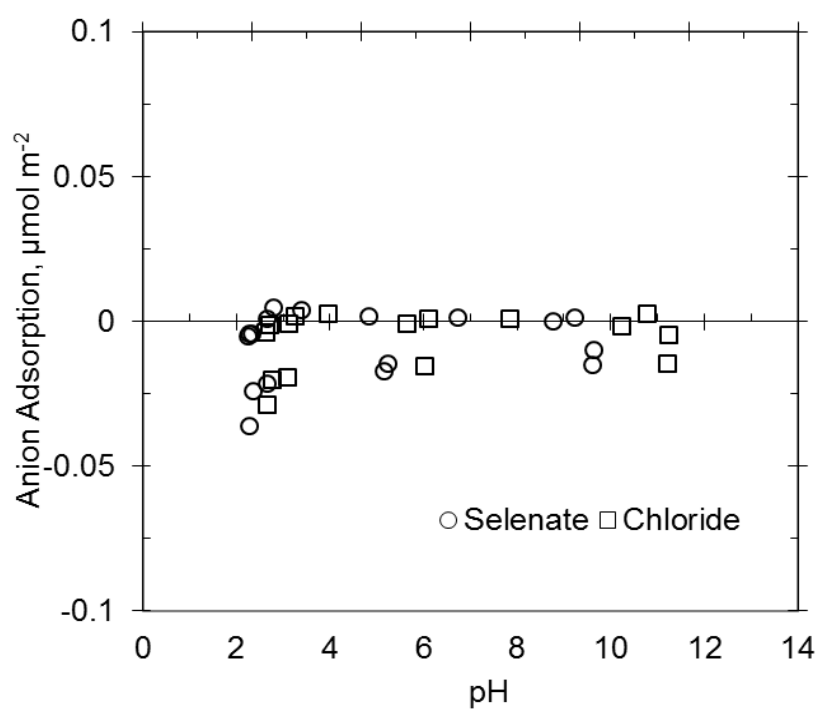
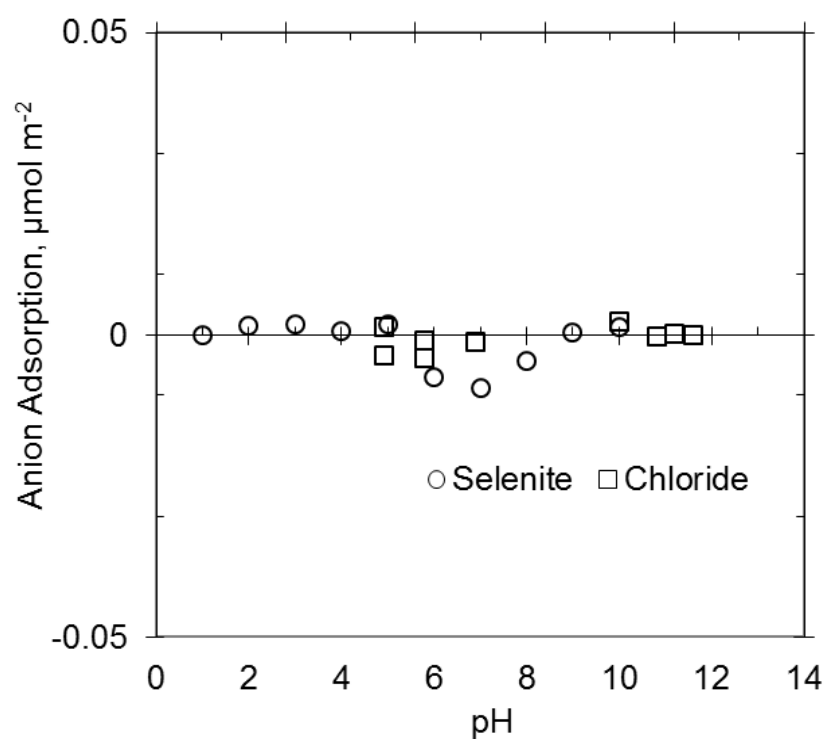
SiO ₂ /Al ₂ O ₃ =23		
Site ID	$\Gamma_{max}(\mu\text{mol m}^{-2})$	pK
1	1.7	1
2	0.3	3
3	0.5	4.9
4	0.5	9
		R ² = 0.993
SiO ₂ /Al ₂ O ₃ =80		
Site ID	$\Gamma_{max}(\mu\text{mol m}^{-2})$	pK
1	0.52	1.3
2	0.26	2.3
3	0.31	6.8
4	0.73	8.8
		R ² = 0.998



Cations	concentrations, mmol L^{-1}
B^{3+}	0.093 ± 0.01
Mn^{2+}	0.114 ± 0.00
Zn^{2+}	0.043 ± 0.01
Fe^{3+}	0.554 ± 0.01
PO_4^{3-}	0.328 ± 0.00







Addendum 2

Raw Data for Chapter Figures

Chapter 2, Figure 2-1. Raw Data

Adsorption envelopes of Na on ZSM-5 differing in $\text{SiO}_2/\text{Al}_2\text{O}_3$ ratio.

Na data on ZSM-5 with SiO₂/Al₂O₃=23
Symbol - circle (○)

Page Ref.	pH	Na Ads, $\mu\text{mol m}^{-2}$
MO-152-1	11.14	2.647115062
MO-153-1	11.12	2.64855696
MO-153-2	10.69	2.569373118
MO-153-3	9.9	2.536697936
MO-153-4	8.25	2.405553886
MO-155-1	8.2	2.403572511
MO-152-2	8.08	2.365773858
MO-153-5	7.55	2.293744827
MO-153'-1	7.36	2.314281159
MO-152-3	7.13	2.246224825
MO-152-4	6.69	2.119042693
MO-155-2	6.66	2.164289034
MO-153-6	6.42	2.048401411
MO-152-5	6.07	2.016942798
MO-152-6	5.27	1.87931306
MO-155-3	5.22	1.936200079
MO-153-7	4.85	1.813797717
MO-152-7	4.57	1.755478793
MO-155-4	4.27	1.656388335
MO-152-8	4.14	1.63772785
MO-153-8	4.12	1.5954075
MO-152-9	3.94	1.551904183
MO-155-5	3.78	1.514954753
MO-153'-2	3.74	1.269818597
MO-152-10	3.68	1.48322465
MO-153-9	3.66	1.449764587
MO-152-11	3.53	1.4024128
MO-155-6	3.5	1.31461543
MO-152-12	3.37	1.301353275
MO-153-10	3.35	1.249068502
MO-153-11	3.3	1.100269972
MO-153'-3	3.28	1.100977634
MO-155-7	3.2	1.18860804
MO-153'-4	3.04	0.966167098
MO-155-8	3.02	1.032755695
MO-153-12	2.95	0.896200178
MO-153-13	2.78	0.851954139
MO-153-14	2.65	0.688054015
MO-152-13	2.55	0.680599426

MO-152-14	2.24	0.349700562
MO-152-15	2.05	0.220920749
MO-153-15	1.83	0.089063483
MO-152-16	1.6	-0.024754877
MO-153-16	1.23	-0.182244176

Na data on ZSM-5 with SiO₂/Al₂O₃=80

Symbol – triangle (□)

(Figure 3: SSSAJ 2011 – Dan Ferreira data for ZSM-5)

Page Ref.	pH	Na Ads, μmol m⁻²
DRF-174-1	10.46	1.4001
DRF-174-2	10.39	1.3561
DRF-174-3	10.03	1.2742
DRF-174-4	9.58	1.1601
DRF-176-1b	9.52	1.1268
DRF-176-2b	9.24	1.049
DRF-176-3b	8.77	0.9575
DRF-176-4b	7.78	0.8685
DRF-179-1	6.53	0.8009
DRF-176-5b	6.15	0.7647
DRF-179-2	4.95	0.7255
DRF-179-3	4.37	0.6823
DRF-176-6b	4.22	0.6428
DRF-174-5	3.83	0.5653
DRF-176-7b	3.64	0.5182
DRF-179-4	3.28	0.3828
DRF-179-5	3.05	0.2784
DRF-179-6	2.86	0.202
DRF-176-8b	2.65	0.2029
DRF-174-6	2.53	0.1471
DRF-174-7	1.93	0.0457
DRF-174-8	1.65	0.0258

**Chapter 2, Figure 2-2. Raw Data
Evaluation of Adsorption sites.**

K ads. data on ZSM-5**Symbol - circle (○)**

Page Ref.	pH	K Ads, $\mu\text{mol m}^{-2}$
MO-156-1	10.87	2.626079778
MO-154-1	10.55	2.764173001
MO-155-1	10.43	2.590230539
MO-155-2	9.61	2.585827037
MO-156-2	9.22	2.484010997
MO-155-3	8.1	2.459229455
MO-156-3	7.36	2.32746441
MO-155-4	6.81	2.245052491
MO-154-2	6.5	2.226842219
MO-154-3	5.92	2.138849385
MO-154-4	5.44	2.012261931
MO-156-4	5.23	1.987309222
MO-154-5	4.84	1.898657693
MO-154-6	4.29	1.797253315
MO-154-7	3.94	1.69647774
MO-155-5	3.89	1.642033098
MO-154-8	3.73	1.655965799
MO-154-9	3.49	1.594554068
MO-155-6	3.44	1.566484365
MO-154-10	3.27	1.539146888
MO-155-7	3.22	1.459436918
MO-157-1	3.17	1.47130769
MO-154-11	3.15	1.441775864
MO-156-5	3.12	1.25967299
MO-157-2	3.04	1.404343331
MO-154-12	3.03	1.255125253
MO-155-8	3.01	1.402254934
MO-157-3	2.93	1.394715562
MO-156-6	2.77	1.272365957
MO-156-7	2.63	1.162570744
MO-156-8	2.48	1.054763851
MO-154-13	2.41	1.02921501
MO-156-9	2.08	0.830337258
MO-156-10	1.91	0.703014666
MO-154-14	1.61	0.334223077
MO-157-4	1.22	0.158548236

Cs ads. data on ZSM-5

Symbol - square (□)

Page Ref.	pH	Cs Ads, $\mu\text{mol m}^{-2}$
MO-157-1	10.73	2.666129162
MO-159-1	10.13	2.546397992
MO-159-2	8.94	2.47463573
MO-161-1	8.44	2.35183725
MO-157-2	6.96	2.256952769
MO-159-3	6.68	2.146749511
MO-161-2	5.66	2.06096957
MO-157-3	5.31	2.054672395
MO-161-3	4.83	1.955270296
MO-159-4	4.58	1.973950893
MO-161-4	4.24	1.848103346
MO-157-4	4.19	1.82504391
MO-159-5	3.76	1.811507345
MO-161-5	3.67	1.688751359
MO-157-5	3.45	1.703128883
MO-161-6	3.45	1.672964211
MO-159-6	3.31	1.69218991
MO-157-6	3.12	1.649686789
MO-159-7	2.88	1.543199775
MO-157-7	2.86	1.547749775
MO-157-8	2.58	1.429227375
MO-157-9	2.3	1.266254186
MO-159-8	2.05	1.113864668
MO-159-9	2	0.990660383
MO-157-10	1.53	0.789022606
MO-159-10	1.18	0.562412306

Na+Cs summation data**Symbol - triangle (△)**

Page Ref.	pH	Na+Cs Ads, $\mu\text{mol m}^{-2}$
MO-157-1	10.73	2.666129
MO-159-1	10.13	2.546398
MO-159-2	8.94	2.474636
MO-161-1	8.44	2.351837
MO-157-2	6.96	2.256953
MO-159-3	6.68	2.14675
MO-161-2	5.66	2.06097
MO-157-3	5.31	2.054672
MO-161-3	4.83	1.95527

MO-159-4	4.58	1.973951
MO-161-4	4.24	1.848103
MO-157-4	4.19	1.825044
MO-159-5	3.76	1.811507
MO-161-5	3.67	1.688751
MO-157-5	3.45	1.703129
MO-161-6	3.45	1.672964
MO-159-6	3.31	1.69219
MO-157-6	3.12	1.649687
MO-159-7	2.88	1.5432
MO-157-7	2.86	1.54775
MO-157-8	2.58	1.429227
MO-157-9	2.3	1.266254
MO-159-8	2.05	1.113865
MO-159-9	2	0.99066
MO-157-10	1.53	0.789023
MO-159-10	1.18	0.562412

Na+K+Cs summation data

Symbol - diamond

Page Ref.	pH	Na+K+Cs Ads, $\mu\text{mol m}^{-2}$
MO-163c-1	12.25	3.204559206
MO-163c-2	12.01	2.995583861
MO-163c-3	11.15	3.024259848
MO-163c-4	10.68	2.491149621
MO-163b-1	7.12	2.390115748
MO-163c-5	5.91	2.038753388
MO-163b-2	4.26	2.007067229
MO-163b-3	3.17	1.551724623
MO-163b-4	2.58	1.402157215
MO-163b-5	2.34	1.372096086
MO-163b-6	2.17	1.328247399
MO-163c-6	2.07	1.100811437
MO-163b-7	1.5	0.935233983
MO-163b-8	1.26	0.574229096

Chapter 2, Figure 2-3. Raw Data

Single ion-exchange adsorption of Na, K and Cs on ZSM-5.

Na ads. Data
Symbol – red circle (○)

Page Ref.	pH	Na Ads, $\mu\text{mol m}^{-2}$	HCl, mL
MO-152-1	11.14	2.647115062	0
MO-153a-1	11.12	2.64855696	0
MO-153a-2	10.69	2.569373118	0.5
MO-153a-3	9.9	2.536697936	0.9
MO-153a-4	8.25	2.405553886	1
MO-155-1	8.2	2.403572511	1
MO-152-2	8.08	2.365773858	1
MO-153a-5	7.55	2.293744827	1.2
MO-153b-1	7.36	2.314281159	1
MO-152-3	7.13	2.246224825	1.1
MO-152-4	6.69	2.119042693	1.2
MO-155-2	6.66	2.164289034	1.2
MO-153a-6	6.42	2.048401411	1.4
MO-152-5	6.07	2.016942798	1.3
MO-152-6	5.27	1.87931306	1.4
MO-155-3	5.22	1.936200079	1.4
MO-153a-7	4.85	1.813797717	1.6
MO-152-7	4.57	1.755478793	1.5
MO-155-4	4.27	1.656388335	1.6
MO-152-8	4.14	1.63772785	1.6
MO-153a-8	4.12	1.5954075	1.8
MO-152-9	3.94	1.551904183	1.7
MO-155-5	3.78	1.514954753	1.8
MO-153b-2	3.74	1.269818597	2
MO-152-10	3.68	1.48322465	1.8
MO-153a-9	3.66	1.449764587	2
MO-152-11	3.53	1.4024128	1.9
MO-155-6	3.5	1.31461543	2
MO-152-12	3.37	1.301353275	2
MO-153a-10	3.35	1.249068502	2.2
MO-153a-11	3.3	1.100269972	2.4
MO-153b-3	3.28	1.100977634	2.2
MO-155-7	3.2	1.18860804	2.2
MO-153b-4	3.04	0.966167098	2.4
MO-155-8	3.02	1.032755695	2.4
MO-153a-12	2.95	0.896200178	2.6
MO-153a-13	2.78	0.851954139	2.8
MO-153a-14	2.65	0.688054015	3

MO-152-13	2.55	0.680599426	3
MO-152-14	2.24	0.349700562	4
MO-152-15	2.05	0.220920749	5
MO-153a-15	1.83	0.089063483	8
MO-152-16	1.6	-0.024754877	10
MO-153a-16	1.23	-0.182244176	20

K ads. Data

Symbol – black triangle (▴)

Page Ref.	pH	K Ads, μmol m⁻²	HCl, mL
MO-156-1	10.87	2.626079778	0
MO-154-1	10.55	2.764173001	0
MO-155-1	10.43	2.590230539	0.4
MO-155-2	9.61	2.585827037	0.6
MO-156-2	9.22	2.484010997	0.7
MO-155-3	8.1	2.459229455	0.8
MO-156-3	7.36	2.32746441	0.9
MO-155-4	6.81	2.245052491	1
MO-154-2	6.5	2.226842219	1
MO-154-3	5.92	2.138849385	1.1
MO-154-4	5.44	2.012261931	1.2
MO-156-4	5.23	1.987309222	1.2
MO-154-5	4.84	1.898657693	1.3
MO-154-6	4.29	1.797253315	1.4
MO-154-7	3.94	1.69647774	1.5
MO-155-5	3.89	1.642033098	1.5
MO-154-8	3.73	1.655965799	1.6
MO-154-9	3.49	1.594554068	1.7
MO-155-6	3.44	1.566484365	1.7
MO-154-10	3.27	1.539146888	1.8
MO-155-7	3.22	1.459436918	1.9
MO-157-1	3.17	1.47130769	1.9
MO-154-11	3.15	1.441775864	1.9
MO-156-5	3.12	1.25967299	2
MO-157-2	3.04	1.404343331	2
MO-154-12	3.03	1.255125253	2
MO-155-8	3.01	1.402254934	2
MO-157-3	2.93	1.394715562	2.1
MO-156-6	2.77	1.272365957	2.2
MO-156-7	2.63	1.162570744	2.4
MO-156-8	2.48	1.054763851	2.8

MO-154-13	2.41	1.02921501	3
MO-156-9	2.08	0.830337258	4
MO-156-10	1.91	0.703014666	5
MO-154-14	1.61	0.334223077	10
MO-157-4	1.22	0.158548236	20

Cs ads. Data

Symbol - blue square (□)

Page Ref.	pH	Cs Ads, $\mu\text{mol m}^{-2}$	HCl, mL
MO-157-1	10.73	2.666129162	0
MO-159-1	10.13	2.546397992	0.5
MO-159-2	8.94	2.47463573	0.8
MO-161-1	8.44	2.35183725	0.9
MO-157-2	6.96	2.256952769	1
MO-159-3	6.68	2.146749511	1.1
MO-161-2	5.66	2.06096957	1.2
MO-157-3	5.31	2.054672395	1.2
MO-161-3	4.83	1.955270296	1.3
MO-159-4	4.58	1.973950893	1.3
MO-161-4	4.24	1.848103346	1.4
MO-157-4	4.19	1.82504391	1.4
MO-159-5	3.76	1.811507345	1.5
MO-161-5	3.67	1.688751359	1.5
MO-157-5	3.45	1.703128883	1.6
MO-161-6	3.45	1.672964211	1.6
MO-159-6	3.31	1.69218991	1.7
MO-157-6	3.12	1.649686789	1.8
MO-159-7	2.88	1.543199775	2
MO-157-7	2.86	1.547749775	2
MO-157-8	2.58	1.429227375	2.5
MO-157-9	2.3	1.266254186	3
MO-159-8	2.05	1.113864668	4
MO-159-9	2	0.990660383	8
MO-157-10	1.53	0.789022606	10
MO-159-10	1.18	0.562412306	20

Additional Information	
ZSM-5 surface area, g m ⁻²	425
ZSM-5 solid concentration, mg L ⁻¹	13.321
Native Na concentrations mmol L ⁻¹	0.232
Concentration of HCl, mol L ⁻¹	0.25
Sample volume, mL	0.035
Off set for Na alone mmol L ⁻¹	0.04
Final concentrations in sample, mmol L ⁻¹	
Na ⁺ alone	20.658
K ⁺ alone	19.716
Cs ⁺ alone	20.118

Chapter 2, Figure 2-4. Raw Data**Two- and three-way competition of Na w/ K, Na w/ Cs, Na w/ K and Cs on ZSM-5.****Na with K, Data****Symbol - red solid circle (●)**

Page Ref.	pH	Na Ads, $\mu\text{mol m}^{-2}$	HCl, mL
MO-156-1	11.9	0.769224	0
MO-157-1	10.44	0.583223	3.3
MO-156-2	10.07	0.543613	3.5
MO-157-2	9.93	0.54392	3.6
MO-157-3	8.5	0.458292	3.8
MO-156-3	6.78	0.427081	4
MO-157-4	6.48	0.388583	4.1
MO-156-4	5.5	0.319383	4.2
MO-156-5	4.34	0.30936	4.4
MO-156-6	3.81	0.219287	4.6
MO-163a-1	3.38	0.23748	5
MO-156-7	3.04	0.147526	5
MO-163a-2	2.54	0.157432	6
MO-163a-3	1.96	0.097997	8
MO-156-8	1.69	0	10
MO-163a-4	1.67	0	10

Additional Information	
ZSM-5 surface area, g m^{-2}	425
ZSM-5 solid concentration, mg L^{-1}	13.321
Native Na concentrations mmol L^{-1}	0.232
Concentration of HCl, mol L^{-1}	0.25
Sample volume, mL	0.035
No off set for competitions	0
Final concentrations in sample, mmol L^{-1}	
Na^+ (Na with K)	20.993
Na^+ (Na with Cs)	20.46
Na^+ (Na with K and Cs)	20.823
K^+ (K with Na)	20.49
K^+ (K with Na and Cs)	20.312
Cs^+ (Cs with Na)	20.034
Cs^+ (Cs with Na and K)	20.239

Na with Cs Data**Symbol - black solid circle (●)**

Page Ref.	pH	Na Ads, $\mu\text{mol m}^{-2}$	HCl, mL
MO-159-1	11.98	0.74431505	0
MO-161-1	11.82	0.571007077	0
MO-161-2	10.42	0.376978978	3.5
MO-159-2	10.37	0.46988296	3.5
MO-161-3	8.61	0.208368489	4
MO-159-3	7.43	0.355717576	4
MO-161-4	6.35	0.227911314	4.2
MO-159-4	5.82	0.138218082	4.2
MO-161-5	5.11	0.122441672	4.4
MO-159-5	4.43	0.107516295	4.4
MO-161-6	4.03	0.083027163	4.6
MO-159-6	3.88	0.248029525	4.6
MO-161-7	3.23	0.08167168	5
MO-159-7	3.06	0.301403881	5
MO-161-8	1.77	0	10
MO-159-8	1.76	0	10

Na with K and Cs Data**Symbol - blue solid circle (●)**

Page Ref.	pH	Na Ads, $\mu\text{mol m}^{-2}$	HCl, mL
MO-163c-1	12.25	0.252013889	0
MO-163c-2	12.01	0.239157004	3
MO-163c-3	11.15	0.262425714	5
MO-163c-4	10.68	0.085681858	6
MO-163b-1	7.12	0.156955578	7
MO-163c-5	5.91	0.046317959	7.3
MO-163b-2	4.26	0.159008067	7.5
MO-163b-3	3.17	0.057521085	8
MO-163b-4	2.58	0.047670655	8.5
MO-163b-5	2.34	0.067401848	9
MO-163b-6	2.17	0.083468724	9.5
MO-163c-6	2.07	0	10
MO-163b-7	1.5	0.072008152	10
MO-163b-8	1.26	0	20

K with Na Data**Symbol - red solid triangle (▲)**

Page Ref.	pH	K Ads, $\mu\text{mol m}^{-2}$	HCl, mL
MO-156-1	11.9	2.1654841	0
MO-157-1	10.44	2.01093709	3.3
MO-156-2	10.07	2.015522332	3.5
MO-157-2	9.93	1.962320538	3.6
MO-157-3	8.5	1.901445831	3.8
MO-156-3	6.78	1.835010151	4
MO-157-4	6.48	1.722206022	4.1
MO-156-4	5.5	1.670329407	4.2
MO-156-5	4.34	1.560533823	4.4
MO-156-6	3.81	1.421323807	4.6
MO-163a-1	3.38	1.192766375	5
MO-156-7	3.04	1.247844432	5
MO-163a-2	2.54	0.917444632	6
MO-163a-3	1.96	0.653295554	8
MO-156-8	1.69	0.608889625	10
MO-163a-4	1.67	0.46890773	10

K with Na and Cs Data**Symbol - blue solid triangle (▲)**

Page Ref.	pH	K Ads, $\mu\text{mol m}^{-2}$	HCl, mL
MO-163b-1	7.12	0.573667637	0
MO-163b-2	4.26	0.442174908	3
MO-163b-3	3.17	0.253828227	5
MO-163b-4	2.58	0.209863908	6
MO-163b-5	2.34	0.201675364	7
MO-163b-6	2.17	0.19261796	7.3
MO-163b-7	1.5	0.107463202	7.5
MO-163b-8	1.26	0.002690693	8
MO-163c-1	12.25	0.911780168	8.5
MO-163c-2	12.01	0.868920726	9

MO-163c-3	11.15	0.873547345	9.5
MO-163c-4	10.68	0.671070011	10
MO-163c-5	5.91	0.489216561	10
MO-163c-6	2.07	0.197462616	20

Cs with Na Data

Symbol - black solid square (■)

Page Ref.	pH	Cs Ads, $\mu\text{mol m}^{-2}$	HCl, mL
MO-159-1	11.98	2.387611	0
MO-161-1	11.82	2.344641	0
MO-161-2	10.42	2.254122	3.5
MO-159-2	10.37	2.236055	3.5
MO-161-3	8.61	2.061893	4
MO-159-3	7.43	2.063934	4
MO-161-4	6.35	1.961642	4.2
MO-159-4	5.82	1.836895	4.2
MO-161-5	5.11	1.757635	4.4
MO-159-5	4.43	1.673766	4.4
MO-161-6	4.03	1.613959	4.6
MO-159-6	3.88	1.631051	4.6
MO-161-7	3.23	1.413125	5
MO-159-7	3.06	1.488546	5
MO-161-8	1.77	0.819255	10
MO-159-8	1.76	0.750786	10

Cs with Na and K Data

Symbol - blue solid square (■)

Page Ref.	pH	Cs Ads, $\mu\text{mol m}^{-2}$	HCl, mL
MO-163c-1	12.25	2.040765	0
MO-163c-2	12.01	1.887506	3
MO-163c-3	11.15	1.888287	5
MO-163c-4	10.68	1.734398	6
MO-163b-1	7.12	1.659493	7
MO-163c-5	5.91	1.503219	7.3
MO-163b-2	4.26	1.405884	7.5
MO-163b-3	3.17	1.140375	8
MO-163b-4	2.58	1.044623	8.5
MO-163b-5	2.34	1.003019	9
MO-163b-6	2.17	0.952161	9.5
MO-163c-6	2.07	0.903349	10

MO-163b-7	1.5	0.755763	10
MO-163b-8	1.26	0.571538	20

Chapter 3, Figure 3-4 to 3-6. Raw Data
Cation Adsorption on Montmorillinite Clay Minerals.

HPLC Data

ICP Data

(shaded)

	10 mmol L ⁻¹ CsCl added	Adsorption or Desorption of Cations (mmol L ⁻¹)				
Page Ref.	% Clay Packing Density	Cs	Na	K	Ca	Mg
MO-170	0	9.432555556	-13.82314272	0.548923077	0.3779	0.142846
MO-145	10	6.655072027	-8.494402488	0.024717949	0.2249	0.095339089
MO-164	50	7.662931638	-8.36033961	0.436923077	0.099075	0.041693697

	10 mmol L ⁻¹ CsCl and KCl added	Adsorption or Desorption of Cations (mmol L ⁻¹)				
Page Ref.	% Clay Packing Density	Cs	Na	K	Ca	Mg
MO-170	0	9.089393913	-16.94336734	4.191553234	0.727025	0.310445
MO-165	10	7.261981235	-8.778008928	4.519913938	0.40875	0.108238934
MO-166	50	6.927671455	-8.538293752	4.234646766	0.2192	0.199061829

	10 mmol L ⁻¹ CsCl and 5 mmol L ⁻¹ CaCl added	Adsorption or Desorption of Cations (mmol L ⁻¹)				
Page Ref.	% Clay Packing Density	Cs	Na	K	Ca	Mg
MO-170	0	9.254724435	-18.71391905	0.918307692	1.3507	0.404237
MO-168	10	6.689980926	-8.386987905	0.754820513	2.148475	0.251634313
MO-168	50	6.504550591	-8.270784615	0.63925641	2.02835	0.115849094

Additional Information	
Montmorillonite Surface, area g m ⁻²	31.82
Clay content in the sample, g	2
Volume of the column, mL	6.546
pH values	
samples of 0% packing density	7.5
samples of 10% and 50% packing density	7.6
Native concentrations of montmorillonite, mmol L ⁻¹	
Na ⁺	2.52
K ⁺	1.8
Mg ²⁺	3
Ca ²⁺	18

Addendum 1, Figure 1. Raw Data
Desorption of Na from ZSM-5

Na desorption in the presence of K
Symbol - circle (○)

Page Ref.	pH	Ads, $\mu\text{mol m}^{-2}$	HCl, mL
MO-154-1	11.14	-0.01798242	0
MO-156-1	10.87	0.002033421	0
MO-155-1	10.43	-0.015204282	0.4
MO-155-2	9.61	-0.018479628	0.6
MO-156-2	9.22	-0.01652131	0.7
MO-155-3	8.1	-0.019845823	0.8
MO-154-2	8.08	-0.030418232	1
MO-156-3	7.36	-0.018604289	0.9
MO-154-3	7.13	-0.023985863	1.1
MO-155-4	6.81	-0.021230398	1
MO-154-4	6.69	-0.022630271	1.2
MO-154-5	6.07	-0.024797841	1.3
MO-154-6	5.27	-0.026298702	1.4
MO-156-4	5.23	-0.024525914	1.2
MO-154-7	4.57	-0.035616577	1.5
MO-154-8	4.14	-0.031104055	1.6
MO-154-9	3.94	-0.026323168	1.7
MO-155-5	3.89	-0.02635899	1.5
MO-154-10	3.68	-0.032164521	1.8
MO-154-11	3.53	-0.029022118	1.9
MO-155-6	3.44	-0.022497038	1.7
MO-154-12	3.37	-0.028411222	2
MO-155-7	3.22	-0.022129452	1.9
MO-157-1	3.17	-0.031393328	1.9
MO-156-5	3.12	-0.027565481	2
MO-157-2	3.04	-0.034448176	2
MO-155-8	3.01	-0.028578291	2
MO-157-3	2.93	-0.029467023	2.1
MO-156-6	2.77	-0.02585899	2.2
MO-156-7	2.63	-0.026288494	2.4
MO-154-13	2.55	-0.036874302	3
MO-156-8	2.48	-0.026764099	2.8
MO-154-14	2.24	-0.040239961	4
MO-156-9	2.08	-0.026333826	4
MO-156-10	1.91	-0.028515154	5
MO-157-4	1.22	-0.034293293	20

Na desorption in the presence of Cs**Symbol - circle (□)**

Page Ref.	pH	Ads, $\mu\text{mol m}^{-2}$	HCl, mL
MO-157-1	10.73	-0.017294303	0
MO-159-1	10.13	-0.030964228	0.5
MO-159-2	8.94	-0.032613401	0.8
MO-161-1	8.44	-0.025511646	0.9
MO-157-2	6.96	-0.037182444	1
MO-159-3	6.68	-0.044645005	1.1
MO-161-2	5.66	-0.029118085	1.2
MO-157-3	5.31	-0.026497497	1.2
MO-161-3	4.83	-0.028228776	1.3
MO-159-4	4.58	-0.031822455	1.3
MO-161-4	4.24	-0.028442474	1.4
MO-157-4	4.19	-0.026454369	1.4
MO-159-5	3.76	-0.032239442	1.5
MO-161-5	3.67	-0.027877018	1.5
MO-157-5	3.45	-0.026477473	1.6
MO-161-6	3.45	-0.025394148	1.6
MO-159-6	3.31	-0.033416864	1.7
MO-157-6	3.12	-0.03053227	1.8
MO-159-7	2.88	-0.032516391	2
MO-157-7	2.86	-0.036195122	2
MO-157-8	2.58	-0.026165566	2.5
MO-157-9	2.3	-0.027376229	3
MO-159-8	2.05	-0.035886711	4
MO-159-9	2	-0.033609319	58
MO-157-10	1.53	-0.027288433	10
MO-159-10	1.18	-0.038883072	20

Addendum 1, Figure 2 and 3. Raw Data**Adsorption envelopes of Na on ZSM-5 differing in SiO₂/Al₂O₃ ratio.****Na data on ZSM-5 with SiO₂/Al₂O₃=23****Symbol - circle (○)**

Page Ref.	pH	Na Ads, $\mu\text{mol m}^{-2}$
MO-152-1	11.14	2.647115062
MO-153-1	11.12	2.64855696
MO-153-2	10.69	2.569373118
MO-153-3	9.9	2.536697936
MO-153-4	8.25	2.405553886
MO-155-1	8.2	2.403572511
MO-152-2	8.08	2.365773858
MO-153-5	7.55	2.293744827
MO-153'-1	7.36	2.314281159
MO-152-3	7.13	2.246224825
MO-152-4	6.69	2.119042693
MO-155-2	6.66	2.164289034
MO-153-6	6.42	2.048401411
MO-152-5	6.07	2.016942798
MO-152-6	5.27	1.87931306
MO-155-3	5.22	1.936200079
MO-153-7	4.85	1.813797717
MO-152-7	4.57	1.755478793
MO-155-4	4.27	1.656388335
MO-152-8	4.14	1.63772785
MO-153-8	4.12	1.5954075
MO-152-9	3.94	1.551904183
MO-155-5	3.78	1.514954753
MO-153'-2	3.74	1.269818597
MO-152-10	3.68	1.48322465
MO-153-9	3.66	1.449764587
MO-152-11	3.53	1.4024128
MO-155-6	3.5	1.31461543
MO-152-12	3.37	1.301353275
MO-153-10	3.35	1.249068502
MO-153-11	3.3	1.100269972
MO-153'-3	3.28	1.100977634
MO-155-7	3.2	1.18860804
MO-153'-4	3.04	0.966167098
MO-155-8	3.02	1.032755695
MO-153-12	2.95	0.896200178
MO-153-13	2.78	0.851954139

MO-153-14	2.65	0.688054015
MO-152-13	2.55	0.680599426
MO-152-14	2.24	0.349700562
MO-152-15	2.05	0.220920749
MO-153-15	1.83	0.089063483
MO-152-16	1.6	-0.024754877
MO-153-16	1.23	-0.182244176

Na data on ZSM-5 with SiO₂/Al₂O₃=80

Symbol - square (□)

(Figure 3: SSSAJ 2011 – Dan Ferreira data for ZSM-5)

Page Ref.	pH	Na Ads, $\mu\text{mol m}^{-2}$
DRF-174-1	10.46	1.4001
DRF-174-2	10.39	1.3561
DRF-174-3	10.03	1.2742
DRF-174-4	9.58	1.1601
DRF-176-1b	9.52	1.1268
DRF-176-2b	9.24	1.049
DRF-176-3b	8.77	0.9575
DRF-176-4b	7.78	0.8685
DRF-179-1	6.53	0.8009
DRF-176-5b	6.15	0.7647
DRF-179-2	4.95	0.7255
DRF-179-3	4.37	0.6823
DRF-176-6b	4.22	0.6428
DRF-174-5	3.83	0.5653
DRF-176-7b	3.64	0.5182
DRF-179-4	3.28	0.3828
DRF-179-5	3.05	0.2784
DRF-179-6	2.86	0.202
DRF-176-8b	2.65	0.2029
DRF-174-6	2.53	0.1471
DRF-174-7	1.93	0.0457
DRF-174-8	1.65	0.0258

Additional Information : ZSM-5 with SiO₂/Al₂O₃=80	
ZSM-5 surface area, g m ⁻²	425
ZSM-5 solid concentration, mg L ⁻¹	8.37
Sample volume, mL	0.035
Off set for Na alone mmol L ⁻¹	-
Final concentrations in sample, mmol L ⁻¹	
Na ⁺ alone	20

Additional Information: ZSM-5 with SiO₂/Al₂O₃=23	
ZSM-5 surface area, g m ⁻²	425
ZSM-5 solid concentration, mg L ⁻¹	13.321
Native Na concentrations mmol L ⁻¹	0.232
Sample volume, mL	0.035
Off set for Na alone mmol L ⁻¹	0.04
Final concentrations in sample, mmol L ⁻¹	
Na ⁺ alone	20.658

Addendum 1, Figure 4. Raw Data

Column Study

Cs adsorption, symbol - circle (○)

Na adsorption, symbol - circle (□)

Page Ref.	Packing Density	Cs Ads, μmol m ⁻²	Na Ads, μmol m ⁻²
MO-170	0	1.830544286	-2.02529
MO-158	10	1.3390362	-1.6619
MO-150	33	1.393266595	-1.71461
MO-162	50	1.36916813	-1.74758

Additional Information	
Montmorillonite Surface, area g m ⁻²	31.82
Clay content in the sample, g	1
Volume of the volume, mL	6.546
pH values	7.6

Addendum 1, Figure 5. Raw Data
Adsorption of Selenite (SeO₃) and Chloride (Cl) on FER.
Page Ref. MO-54, 62, 68 and 69

pH	SeO₃ ads, $\mu\text{mol m}^{-2}$
9.923	-0.00028014
9.092	-0.004124312
8.92	0.013709366
8.92	0.013709366
8.898	-0.005220394
8.608	0.003778686
8.608	0.003778686
8.56	-0.001000888
8.229	-0.001277764
8.037	0.009074917
8.037	0.009074917
7.947	0.063465572
7.772	0.007481346
7.771	-0.010445683
7.564	0.001445454
6.944	-0.007914633
6.907	0.007435969
6.907	0.007435969
6.717	0.004149586
5.782	-0.001114006
5.737	0.002610023
5.733	-0.010176966
5.107	-0.011592547
5.107	-0.013980689
4.546	-0.000851843
4.489	0.001663361
4.489	0.001663361
4.123	0.001306541
3.674	0.047421363
3.674	-0.019965244
3.589	-0.002271037
3.557	-0.000857772
3.494	-0.000596461
3.494	-0.000596461
3.376	0.000997624
3.349	0.00782755
3.055	0.003488422

3.005	0.000210349
2.967	0.010847805
2.967	0.010847805
2.932	0.004120505
2.9	-0.169513238
2.9	0.002141996
2.865	0.008460217
2.822	0.008263312
2.738	0.008138658
2.738	0.008138658
2.243	0.091160953
2.243	0.140983432
1.9	0.062568081
1.9	-0.019054416
1.7	-0.040670148
1.7	-0.003036189
1.579	-0.022430024
1.579	-0.067611668
1.504	0.063322251
1.504	-0.079267121

pH	Cl Ads, $\mu\text{mol m}^{-2}$
8.608	-0.003263254
8.037	0.000550288
7.772	0.033986686
7.729	0.004807036
7.564	0.006566492
6.97	-0.002428335
6.717	0.018850974
6.556	0.005939312
5.782	-0.005060768
5.737	0.011856961
5.107	-0.018521446
5.107	-0.045415756
4.489	-0.005305755
4.399	0.005028193
4.123	0.005935429
3.674	-0.043806765
3.674	-0.032448936
3.557	-0.003896734
3.525	0.003065463
3.494	-0.005645974

3.349	0.035559439
3.005	0.000955587
2.967	-0.000732601
2.96	-1.25759E-05
2.9	-0.03847416
2.9	0.00948843
2.865	0.038433557
2.851	0.005643444
2.738	-0.018965094
2.243	-0.013555465
2.243	-0.039695989
1.9	-0.036627081
1.7	-0.021396488
1.579	-0.038781382

Additional Information	
FER surface area, g m ⁻²	440
Pore size, nm	0.54 × 0.42 0.48 × 0.35
Concentration of HCl, mol L ⁻¹	0.1
Sample volume, mL	0.035
Selenate, Selenite concentrations, mmol L ⁻¹	6.5

Addendum 1, Figure 6. Raw Data

Adsorption of Selenate (SeO_4) and Chloride (Cl) on FER.

Page Ref. MO-55, 66 and 70.

pH	SeO_4 ads, $\mu\text{mol m}^{-2}$
9.891	-0.014703884
9.634	-0.020385396
9.375	-0.003849749
8.994	-0.00451753
8.383	0.008404366
7.617	-0.01212294
7.268	-0.010089535
5.928	-0.002907124
4.422	0.002415804
3.694	-0.011839509
3.262	0.003923144
2.961	-0.006802159
2.712	0.042186387
2.61	-0.020803775
2.478	0.006607153
2.304	0.045226833
2.202	-0.015391028
2.101	-0.037480953
2.066	0.026843655
2.003	0.022070834
2.002	0.01744803
1.958	0.035996947
1.948	-0.043204645
1.902	-0.017888846

pH	Cl Ads, $\mu\text{mol m}^{-2}$
11.883	0.009426088
10.963	-0.001651514
10.803	-0.001326287
10.75	-0.018098366
9.634	-0.04952146
9.375	-0.039246055
8.994	-0.020317827
8.383	-0.04539177

7.617	-0.034944054
7.268	-0.067797783
6.121	-0.010394285
5.928	-0.018439651
4.967	-0.003692523
4.422	-0.049782797
3.694	-0.02463993
3.262	-0.04810852
3.003	-0.003267141
2.961	-0.015743003
2.947	-0.002213021
2.712	-0.039607905
2.635	0.00494472
2.478	-0.013425436
2.304	-0.04215809
2.202	-0.025225783
2.145	-0.013312707
2.026	-0.001429069
1.88	-0.000864462
1.836	-0.01490751
1.747	-0.015278876
1.528	0.025926937
1.448	-0.035174312

Addendum 1, Figure 7. Raw Data

Adsorption of Selenite (SeO₃) and Chloride (Cl) on FAU.

Page Ref. MO-55, 66 and 70.

pH	SeO₃ ads, $\mu\text{mol m}^{-2}$	Cl Ads, $\mu\text{mol m}^{-2}$
8.293	0.001383363	-0.000127781
8.001	0.001711496	0.000177368
7.729	0.000426371	-0.000309608
7.14	0.00067793	0.002091158
4.925	-0.004404273	-0.001216645
4.14	0.001664477	-0.000854443
4.14	-0.008853058	-0.00387617
3.518	0.001636266	0.001340787
3.518	-0.007081978	-0.003485285

Addendum 1, Figure 7. Raw Data
Adsorption of Selenate (SeO₄) and Chloride (Cl) on FAU.
Page Ref. MO-55, 66 and 70.

pH	SeO₄ ads, $\mu\text{mol m}^{-2}$	Cl Ads, $\mu\text{mol m}^{-2}$
9.637	-0.009952341	-0.004585371
9.608	-0.015232145	-0.014879278
9.243	0.001075195	0.002489181
8.767	0.000148002	-0.001987513
6.73	0.001154516	0.000795354
5.227	-0.014612337	0.000751304
5.164	-0.017326984	-0.015396987
4.842	0.001634073	-0.000839946
3.391	0.00386983	0.002334849
2.787	0.004564619	0.001763504
2.665	0.000701754	-0.001013511
2.653	-0.021602144	-0.01925307
2.37	-0.024018561	-0.020194304
2.329	-0.004362549	-0.001245006
2.275	-0.036145931	-0.028777825
2.268	-0.004279255	-0.003719314
2.256	-0.005026847	-0.001245006

Additional Information	
FAU surface area, g m^{-2}	730
Pore size, nm	0.74×0.72
Concentration of HCl, mol L^{-1}	0.1
Sample volume, mL	0.035
Selenite, Selenate concentrations, mmol L^{-1}	6.5